Rupture area and displacement of past Cascadia great earthquakes from coastal coseismic subsidence

Lucinda J. Leonard[1,†], Claire A. Currie[2], Stéphane Mazzotti[1,3], and Roy D. Hyndman[1,3]
[1]*Geological Survey of Canada, Pacific Geoscience Centre, 9860 West Saanich Road, Sidney, British Columbia V8L 4B2, Canada*
[2]*Department of Physics, University of Alberta, Edmonton, Alberta T6G 2G7, Canada*
[3]*School of Earth and Ocean Sciences, University of Victoria, PO Box 3065 STN CSC, Victoria, British Columbia V8W 3V6, Canada*

ABSTRACT

Coastal marshes record a 6500 yr history of coseismic displacements in great earthquakes at the Cascadia subduction zone. We compiled estimates of coseismic displacement for past megathrust events based on correlations with megathrust-triggered turbidites, and estimated megathrust slip based on comparisons of marsh displacements with dislocation model predictions. Age-correlated marsh data are compatible with event rupture extents defined by the published turbidite record, and a 6500 yr mean recurrence interval that increases northward from ~230 to ~480 yr. Within the constraints of the marsh data, the width of the coseismic rupture zone generally agrees with the downdip width of the interseismic locked zone inferred from geodetic and thermal data. In southernmost Cascadia, where the model does not include the complex deformation near the Mendocino triple junction, the coastal data may be better fit by a model with an ~25% narrower rupture than that inferred from regional geophysical data. At each coastal marsh site, coseismic displacements are roughly similar from event to event, independent of the time since the previous event. Slip in the A.D. 1700 earthquake was consistent with the preceding interval of strain accumulation (~200 yr) only at the northern and southern ends of the margin, but it was apparently much higher in southern Washington and northern Oregon, possibly indicating postseismic contamination and/or catch-up coseismic slip to make up for a deficit in the preceding event. Overall agreement between the dislocation models and the marsh data for most of the margin implies that such models can be usefully applied to rupture and ground shaking predictions.

[†]E-mail: lleonard@nrcan.gc.ca

INTRODUCTION

Southwestern Canada and the northwestern United States are at significant risk from great earthquakes (M > 8) and tsunamis that occur on the Cascadia subduction zone (Fig. 1) approximately every 500 yr (e.g., Atwater and Hemphill-Haley, 1997; Goldfinger et al., 2008). Simulations suggest that a future great earthquake will result in widespread damage to the region; high-rise buildings are particularly at risk from ground shaking (Olsen et al., 2008), and coastal areas are at risk from tsunami inundation (e.g., Geist, 2005; Cherniawsky et al., 2007).

Along much of the Cascadia coast, the subduction earthquake cycle results in gradual interseismic uplift and abrupt coseismic subsidence as the upper plate slowly shortens and upwarps due to locking of the plate interface and then release of the accumulated strain during great earthquakes (e.g., Dragert et al., 1994; Fig. 2). The most recent great earthquake in A.D. 1700 predates the written historical record of the Pacific Northwest, but it resulted in burial of prehistoric hearths and soils (e.g., Minor and Grant, 1996). Buried soils in Cascadia coastal marshes provide an up to 6700-yr-long record of coseismic displacement events (e.g., Atwater and Hemphill-Haley, 1997; Kelsey et al., 2002; Witter et al., 2003). Radiocarbon dating and along-margin stratigraphy of buried soils (e.g., Nelson et al., 2006), tsunami deposits (e.g., Kelsey et al., 2005), and offshore turbidites (e.g., Adams, 1990; Goldfinger et al., 2003, 2008) have been used to establish approximate event frequency and rupture extents. Complementary data on the current rates of interseismic strain come from geodetic measurements that can be used to constrain elastic dislocation fault models (e.g., Hyndman and Wang, 1995; Flück et al., 1997; Wang et al., 2003) and estimate first-order coseismic slip magnitude. However, it is not clear exactly how the pattern of interseismic deformation relates to that of coseismic rupture. Episodic tremor and slip locations also provide a constraint on the downdip limit of rupture (e.g., Kao et al., 2006). Megathrust fault slip can be constrained more directly by comparing the predictions of dislocation models for coastal coseismic vertical displacements with those observed in past events (Leonard et al., 2004).

Leonard et al. (2004) compared coseismic displacements from compiled coastal marsh data for the A.D. 1700 megathrust earthquake with those predicted from elastic dislocation models constrained by geophysical (geodetic, thermal, seismic) data. The study showed that a simple elastic dislocation model of the seismic release of ~550–800 yr of accumulated strain can produce coastal subsidence generally consistent with the marsh data. The exceptions are at the northern and southern ends of the subduction zone, where subsidence in A.D. 1700 was significantly less than that predicted by these models. Based on data available at that time, Leonard et al. (2004) took the penultimate great megathrust event to have occurred ~600–1000 yr prior to the A.D. 1700 earthquake (e.g., Atwater and Hemphill-Haley, 1997). However, turbidite analyses and some coastal data place the penultimate event at only ~200 yr prior to A.D. 1700 (e.g., Goldfinger et al., 2008).

In this paper, we examine older (pre–A.D. 1700) Cascadia great earthquakes and a broader range of fault rupture models, expanding on the preliminary analysis of Hyndman et al. (2005). First, we investigate how the A.D. 1700 earthquake compares with other events spanning a longer time period. Average estimated rupture and the rupture variability of a number of past events are expected to be better predictors of future great earthquakes than just the last megathrust event. In Cascadia coastal marshes, the buried soil from the A.D. 1700 event is the uppermost in a sequence of up to 14 buried soils (e.g., Nestucca Bay; Darienzo et al., 1994) extending over ~6500 yr. We compile an

GSA Bulletin; November/December 2010; v. 122; no. 11/12; p. 1951–1968; doi: 10.1130/B30108.1; 11 figures; 1 table; Data Repository item 2010076.

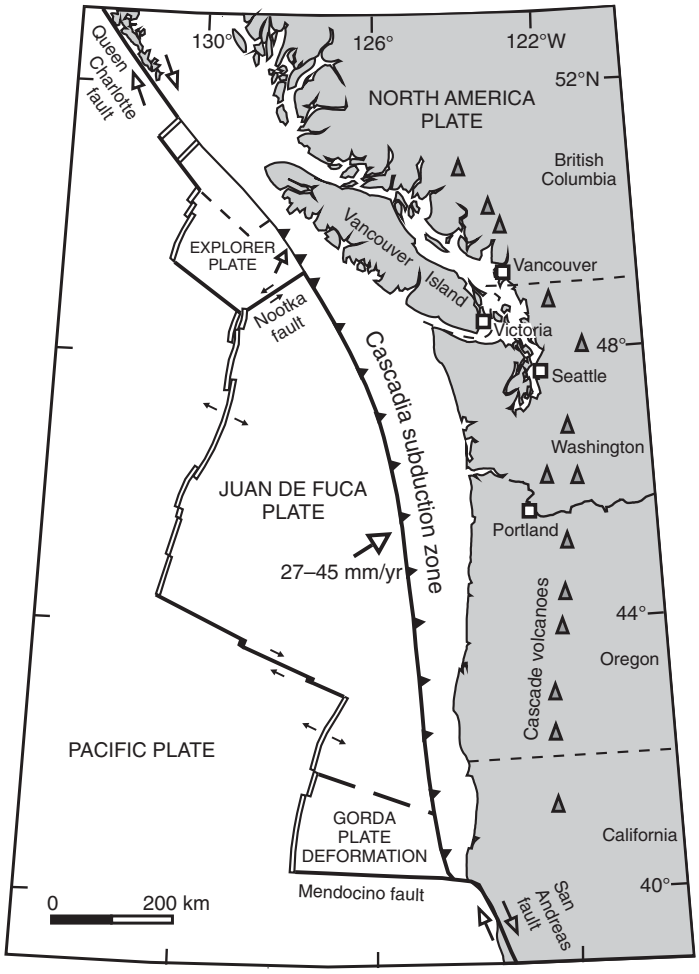

Figure 1. Plate-tectonic setting of the Cascadia subduction zone. The study covers the Juan de Fuca–North America plate boundary from the Mendocino fault in the south to the Nootka fault in the north. Tectonic deformation is complex at the southern and northern ends of the subduction zone. In this study, the Explorer plate subduction in the north is assumed to be independent.

extensive data set of radiocarbon ages and/or coseismic displacement estimates for buried soils and tsunami deposits (GSA Data Repository Table DR1[1]) at sites spanning most of the Cascadia coast in northern California, Oregon, Washington, and British Columbia (Fig. 3). Based mainly on the megathrust event history established by Goldfinger et al. (2008), we estimate along-margin patterns of coastal coseismic displacement and infer megathrust slip for individual correlated events. We test a range of simple elastic dislocation models, considering variations in earthquake slip, rupture width, and rupture length (segmented ruptures). We also consider possible effects of transient fault behavior (e.g., postseismic slip and viscous relaxation), although there is limited constraint on these behaviors.

CASCADIA COASTAL MARSH COSEISMIC DATA

Estimation of Coseismic Subsidence from Paleoseismic Data

The great earthquake cycle has led to the formation of repeated buried peat-mud couplets in marsh sediments along the Cascadia coast. Coseismic subsidence drops high marsh/upland soils into lower intertidal zones to become "buried soils," which are subsequently overlain by muddier sediments. During a sufficiently long interseismic period, gradual uplift and sediment buildup bring the marsh surface back to a higher intertidal zone, facilitating the development of a new organic-rich soil. Each intertidal zone is characterized by both its organic content and a distinct assemblage of plants, diatoms, and foraminifera, all of which are dependent on elevation, mainly controlled by relative tolerance to tidal exposure.

Coseismic subsidence estimates are compiled here, and additional estimates have been made using published stratigraphic and sedimentological data, as described in detail by Leonard et al. (2004). The magnitude of coseismic subsidence is the difference in paleoelevation between each buried soil and the sediment immediately overlying it, which we assume captures the paleoelevation prior to postseismic displacement, i.e., the elevation immediately after the event. In most cases, the deposition of low intertidal muddy sediments over the dropped soil is expected to occur within a few weeks of a megathrust earthquake (e.g., Ovenshine and Kachadoorian, 1976), thus leaving little time for significant postseismic displacement.

Paleoelevation is estimated by comparing the elevation-dependent characteristics of the buried sediment (organic content, macrofossils, and microfossil assemblages) with sediment characteristics of modern intertidal elevational zones. The fossil characteristics are matched with a particular intertidal zone to provide a paleoelevation range. The error on the coseismic subsidence estimates is primarily due to the width of the distinct intertidal zones. Most published data are confined to organic content (e.g., peat, peaty mud) and sometimes macrofossils (e.g., spruce stumps, Triglochin rhizomes), leading to coseismic subsidence estimate uncertainties of typically ±0.5–0.8 m, but some also include detailed microfossil analyses, generally leading to higher precision. Transfer function analysis of foraminifera, diatoms, and/or pollen, incorporating modern training data sets, can reduce uncertainties to ±0.2–0.3 m (e.g., Hughes et al., 2002; Hawkes et al., 2008; Nelson et al., 2008). There have been many studies of buried soils along the Cascadia margin (sites shown on Fig. 3). The measurement and reporting methods vary, as do the details of the interpretations, and we grade the estimates into three quality levels (Table DR1 [see footnote 1]).

Cascadia Megathrust Earthquake History

The most recent great Cascadia earthquake affected the entire margin from northern California to central Vancouver Island (Fig. 3). The

[1]GSA Data Repository item 2010076, compilation of coseismic displacement and radiocarbon data for Cascadia great earthquakes (Tables DR1–DR3), is available at http://www.geosociety.org/pubs/ft2010.htm or by request to editing@geosociety.org.

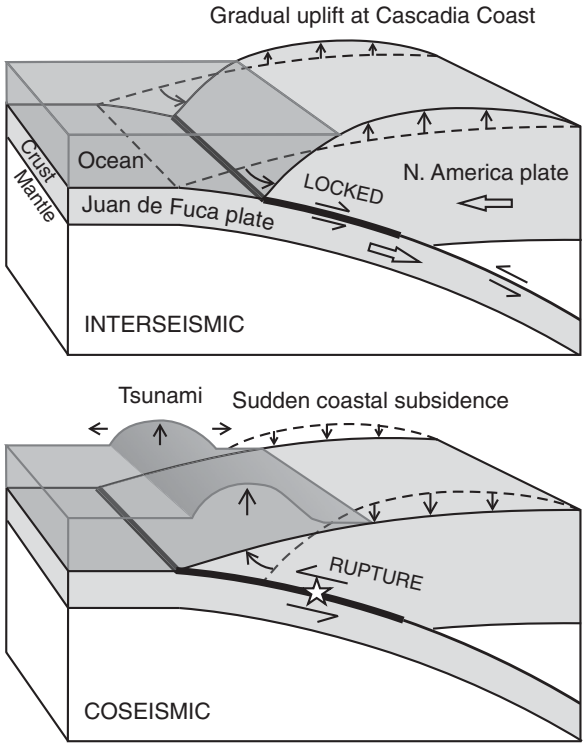

Figure 2. Pattern of interseismic and coseismic deformation associated with a subduction thrust fault (modified from Atwater et al., 2005). Note that the magnitude of uplift/subsidence varies with distance from the locked/rupture zone.

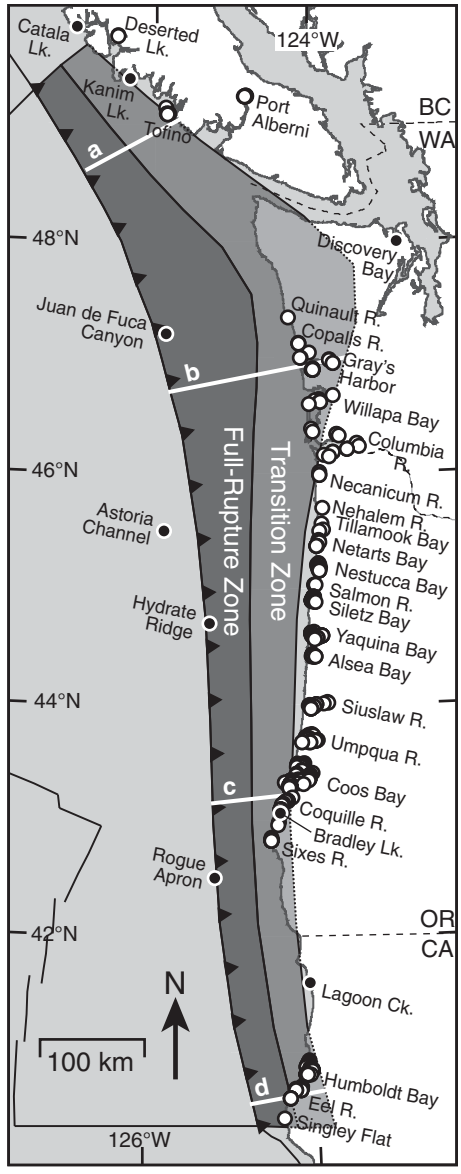

Figure 3. Location of coastal data sites relative to the full-rupture (dark gray) and transition (medium gray) zones. White-filled circles—buried soil sites. Black-filled circles—tsunami/turbidite deposit sites. White lines labeled a–d show locations of profiles in Figures 9 and 11.

date of this event (26 January 1700), determined from a far-field tsunami documented in Japan (Satake et al., 1996), is consistent with tree-ring studies constraining tree submergence to between the 1699 and 1700 growth seasons (Yamaguchi et al., 1997) and Native American oral records of a shaking and flooding event between 1690 and 1715 (Ludwin et al., 2005).

Buried soils at Cascadia represent a sequence of events over the past ~6500 yr (Fig. 4). The length of the record is determined by the regional pattern of sea-level change in the late Holocene. We assume that the buried soils result from coseismic subsidence during subduction zone earthquakes (see discussion in Nelson et al., 1996a). Correlation of buried soils is often possible within individual or closely located estuaries, generally by "bar-code" matching (e.g., Atwater and Hemphill-Haley, 1997), but large uncertainties in radiocarbon ages make correlation problematic over greater onshore distances. In most cases, calibrated radiocarbon ages represent maximum limiting ages (age of detrital material within buried soils that must predate the soil itself as well as the coseismic displacement); closely limiting ages can be provided by dating of growth-position fossils in the buried soil (close maximum) or in the overlying sediment (rhizomes of colonizing plants; close minimum) (e.g., Atwater et al., 2004a).

Atwater et al. (2004a, 2004b) correlated buried soils in southern Washington and northernmost Oregon using a combination of high-precision radiocarbon data to produce an ~4000 yr time line of plate-boundary earthquakes in that region (vertical bars under "SW WA/NW OR" in Fig. 4). Earthquake and/or tsunami histories have also been estimated at other estuaries and/or coastal lakes in Oregon (Kelsey et al., 2002, 2005; Nelson et al., 1996b, 2004, 2008; Witter et al., 2003) and northern California (Garrison-Laney et al., 2006; Patton and Witter, 2006).

Coastal marshes on Vancouver Island, British Columbia, preserve only the A.D. 1700 buried soil and one previous tsunami deposit (Fig. 4) above older bedrock or Pleistocene sediments, but some older events are preserved as tsunami deposits in coastal lakes, with limited, generally unquantifiable microfossil evidence for coseismic subsidence (Hutchinson et al., 1997, 2000; Clague et al., 1999). One explanation for the lack of older buried soils is long-term local tectonic uplift at a rate faster than eustatic sea-level rise (e.g., Bindoff et al., 2007), such that the previous earthquake records have been erased by erosion/bioturbation. Compilations of Holocene relative sea-level changes (Friele and Hutchinson, 1993; Hutchinson et al., 1997, 2000) indicate that the west coast of Vancouver Island has been rising in the late Holocene, with a relative sea-level fall of ~1–1.5 mm/yr. Long-term tectonic uplift could relate to the behavior of the megathrust fault, which may be complex in this area due to the proximity of the Nootka fault and adjacent young Explorer plate (Fig. 1).

A correlated "event" based solely on the onshore buried soil record could represent rupture of the entire margin in one megathrust earthquake. However, events that appear to have similar ages at different sites may result from different earthquakes on adjacent segments separated by days (e.g., Solomon Islands: M 8.0 and 8.1, July 1971; Lay and Kanamori, 1980),

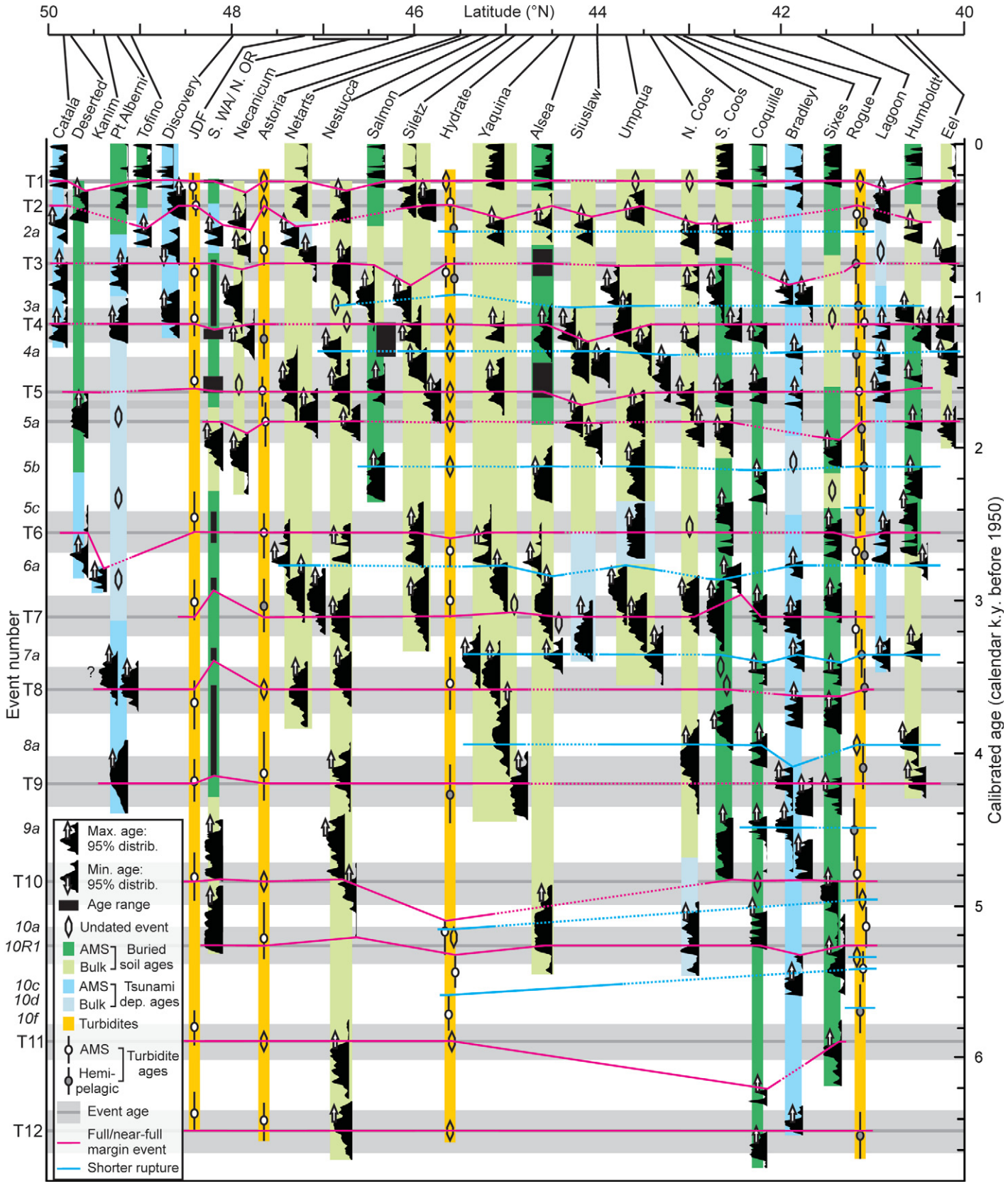

Figure 4. Age ranges and proposed correlations of Cascadia plate-boundary events plotted against latitudinal position. Site locations are shown in Figure 3. Ages plotted are the calibrated age distributions (at least 95% confidence, normalized to uniform width) calculated from published radiocarbon ages using OxCal (version 4.0; Bronk Ramsey, 2001) with the INTCAL04 terrestrial calibration curve (Reimer et al., 2004). Radiocarbon data for buried soil and tsunami deposit horizons are given in Tables DR1 and DR2 (see text footnote 1), respectively. Where possible, ages from two or more cores at the same locality are combined using the R_Combine feature of OxCal (Table DR3 [see text footnote 1]). The ages plotted for events 1, 3, 6,7, 8, and 9 in the southwest Washington/northwest Oregon compilation represent the approximate time of death of trees and/or shrubs, and those for events 4 and 5 are bracketed by time of death of trees in the buried soil and age of colonizing plants in overlying sediment (Atwater et al., 2004a). Rectangles for events 3 and 5 at Alsea Bay, and event 4 at Salmon River, are similarly bracketed ages (Nelson et al., 2004, 2008). Vertical bars link successive events at each site (green—buried soils; blue—tsunami deposits; orange—selected turbidite deposits). Darker shading is for accelerator mass spectrometry (AMS) ages on plant material; lighter shading is for less accurate bulk peat dating. Turbidite ages are AMS ages on planktonic foraminifera corrected for marine reservoir effects and erosion (white circles) or are inferred ages based on hemipelagic sediment thickness and sedimentation rates (gray circles) (Goldfinger et al., 2008, 2010). White arrow symbols on age probability distributions mark maximum earthquake ages (see text). Open double-pointed symbols show undated events. Where ages overlap within a core, the stratigraphically younger age is placed on the left. Gray horizontal lines and lighter shaded bars show the estimated timing of each full- or near-full-margin turbidite event (best estimate and uncertainty) from Goldfinger et al. (2010). Events labeled T1, T2, T3, etc., represent relatively thick turbidites that are correlated between all core sites; those labeled 2a, 3a, 10R1, etc., represent relatively thin turbidites that correlate among fewer sites. Pink lines correlate data for events with inferred full- or near-full-margin extent; blue lines correlate data for events with more limited along-margin extent. Sources of radiocarbon age data: Catala Lk.—Clague et al. (1999); Deserted Lk.—Hutchinson et al. (2000); Kanim Lk.—Hutchinson et al. (1997); Port Alberni and Tofino—Clague and Bobrowsky (1994a); Discovery Bay—Williams et al. (2005); SW Washington/NW Oregon—events 1, 3–5, 6–9—Atwater et al. (2004a, 2004b); event 2—Atwater and Hemphill-Haley (1997); events 5a, 10, 10R1—Shennan et al. (1996); Necanicum R.—Darienzo et al. (1994); Netarts Bay—Darienzo and Peterson (1990); Shennan et al. (1998); Nestucca Bay—Darienzo et al. (1994); Salmon R.—Nelson et al. (2004); Siletz Bay—Darienzo et al. (1994); Peterson et al. (1996); Yaquina Bay—Darienzo et al. (1994); Alsea Bay—Peterson and Darienzo (1991); Nelson et al. (2008); Siuslaw R.—Nelson (1992a); Briggs (1994); Umpqua R.—Briggs (1994); N. Coos Bay—Nelson (1992a); Briggs (1994); S. Coos Bay—Briggs (1994); Nelson et al. (1996b, 1998); Coquille R.—Nelson (1992a, 1992b); Witter et al. (1997, 2003); Bradley Lk.—Kelsey et al. (2005); Sixes R.—Kelsey et al. (1998, 2002); Lagoon Cr.—Garrison-Laney et al. (2006); Humboldt Bay—Vick (1988); Carver et al. (1992); Clarke and Carver (1992); Valentine (1992); Pritchard (2004); Patton and Witter (2006); Eel R.—Li (1992). Turbidite cores Juan de Fuca (JDF), Astoria, Hydrate, Rogue—Goldfinger et al. (2008, 2010).

months (e.g., Sumatra-Nias: M ~9 December 2004 and M 8.7 March 2005; Banerjee et al., 2007), years (e.g., Tonankai-Nankaido: M 8.2 1944 and M 8.2 1946; Nakanishi et al., 2002), or decades (e.g., Alaska: M 8.2 1938 and M 9.2 1964; McCann et al., 1980). Some buried soils may reflect earthquakes that are not recorded at other sites for various reasons such as: local upper-plate faulting; short plate-boundary segment rupture; or long plate-boundary rupture, but with too short a preceding strain accumulation period to be recorded at most sites. In the case of tsunami deposits, an additional explanation could be a far-field earthquake. Segmentation of plate-boundary events is better investigated with the turbidite record. Detailed correlations suggest that individual earthquakes impart a unique stratigraphic signature (e.g., relative thickness, number of sandy pulses) to turbidites in separate channels spanning large distances (e.g., Goldfinger et al., 2007a, 2008). The turbidite data so far support synchroneity of at least most correlated buried soil events (e.g., Goldfinger et al., 2008).

Witter et al. (2003) and Nelson et al. (2006) correlated events at up to eight sites along the coast from northern California (Lagoon Creek) to Vancouver Island. According to their work, many events appear to have ruptured at least the majority of the margin's 1200 km length, but segmented ruptures have also occurred. This is supported by the turbidite record (Goldfinger et al., 2003, 2008), which discriminates between full- or near-full-margin events (T1, T2, T3, etc. in Fig. 4) and thinner turbidites (2a, 3a, 4a, etc. in Fig. 4) that span varying lengths of the southern part of the margin (sometimes as far north as northern Oregon). Goldfinger et al. (2008) suggested that segment boundaries occur at three forearc structural highs in Oregon. In a later section, we investigate such segmented ruptures and their expected patterns of coseismic subsidence.

We have compiled radiocarbon ages from the literature, making a distinction between ages of differing quality (Fig. 4). Using the turbidite event time line and correlations of Goldfinger et al. (2008, 2010), we assigned buried soils to events with similar ages, and compiled subsidence data for individual events (Fig. 5). Some correlations are uncertain and have alternate interpretations. Some ages appear to better match a different event than the one correlated, but we attempt to provide the simplest set of correlations that are in keeping with the radiocarbon age limits. Undated soils and tsunami deposits are correlated according to their position in sequence. Each full- or near-full-margin event in the turbidite record has a correlative in the buried soil record, but some of the shorter ruptures inferred by thinner turbidites do not appear to have an onshore record; ~14% of events in the past 5000 yr and ~25% in the past 6500 yr appear to be missing onshore (Fig. 4).

Over the last ~6500 yr, the average recurrence interval of megathrust earthquakes in southern Cascadia is ~230 yr (Goldfinger et al., 2008, 2010). Recurrence intervals increase to ~570 yr in northern Cascadia; with no apparent independent ruptures in the north, this is also the average recurrence for events that produced turbidites along the full or near-full length of the margin (main events T1 to T12 in Fig. 4). The buried soil record suggests that two additional events (5a and 10R1) ruptured the margin as far north as Gray's Harbor, Washington (~47°N; Fig. 3). This is the northernmost buried soil locality with a long pre–1700 record (Fig. 4), so these events could extend to off Vancouver Island. Incorporating these events reduces the average recurrence of near-full-margin ruptures, or at least of events at 47°N, to ~480 yr. Events 5a and 10R1 did not generate observable turbidites at Juan de Fuca canyon (Fig. 3), implying that significant shaking did not occur within ~90 km of the canyon head at ~48°N (maximum triggering distance estimated by Goldfinger et al., 2007a). However, an event with a similar age to event 10R1

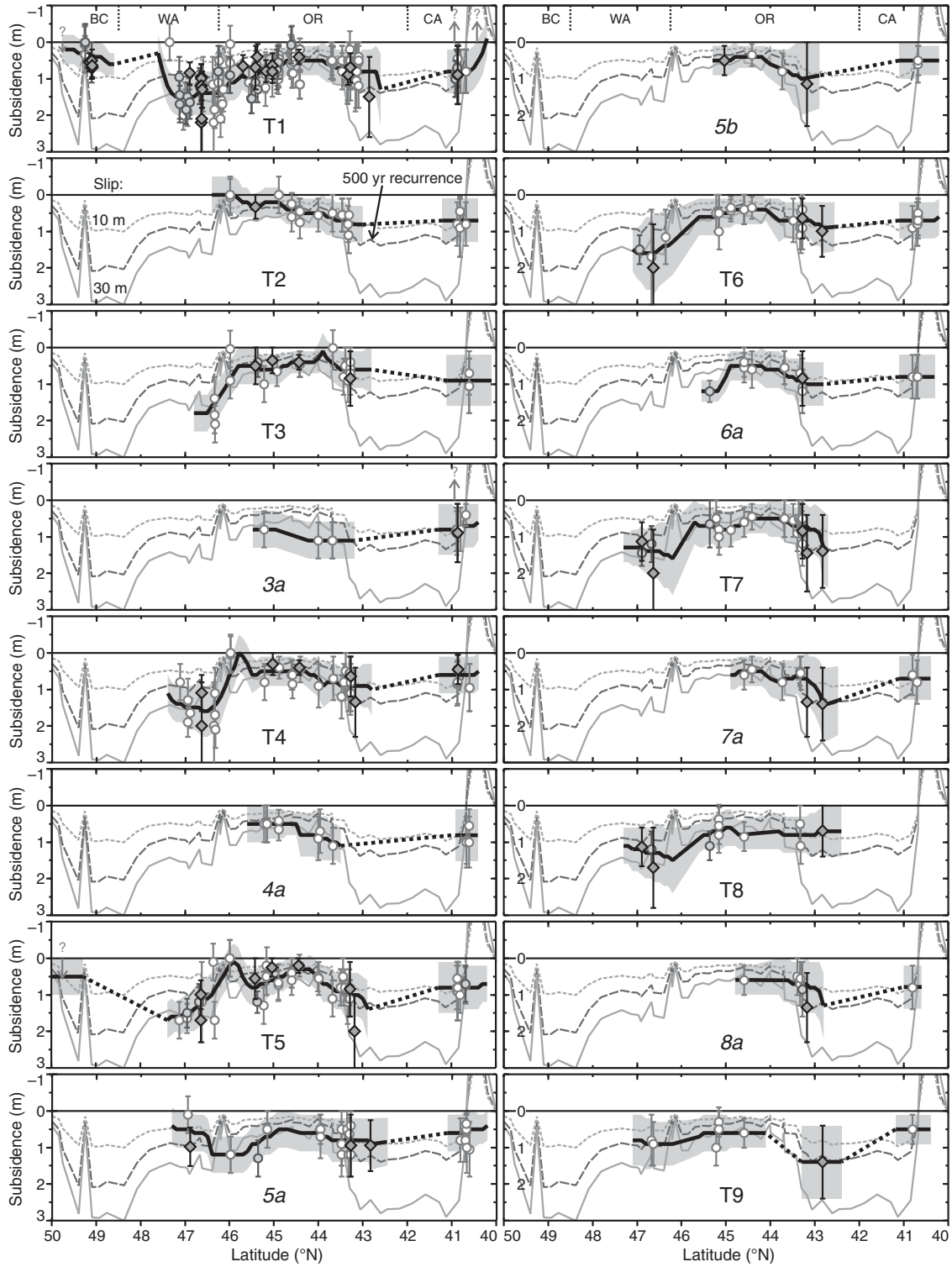

Figure 5. Estimated coseismic subsidence in events 1–9 (T1–T9), as correlated in Figure 4, plotted against latitude (data details in Table DR1 [see footnote 1]). Gray diamonds represent high-quality estimates from statistical microfossil analyses; gray circles are medium-quality estimates from relative organic content, with macrofossil data on both sides of the contact and/or relative fresh/brackish diatom concentration; white circles are low-quality estimates from relative organic content, with macrofossil data for one/no sides of the contact. Thick black lines and gray shading represent the weighted average (moving average over 1°) and uncertainty, respectively, of estimated coseismic subsidence. Upward/downward arrows with question marks indicate unquantifiable estimates of uplift/subsidence. Thinner lines (labeled for event 2) show the predicted subsidence for megathrust slip of 10 m and 30 m (light-gray lines) and for the release of 500 yr of accumulated strain (dark-gray dashed line). See Table 1 for data sources.

(5270–5310 yr B.P.) did trigger a debris flow at Effingham Inlet, western Vancouver Island (~49°N; R. Enkin, 2009, personal commun.). Debris flows off southern Vancouver Island could also correlate with events 5a (Saanich Inlet, ~48.5°N: 1831–2006 yr B.P.; Blais-Stevens et al., 2009) and 5b (2180–2399 yr B.P. at Saanich Inlet; Blais-Stevens et al., 2009; and 2161–2185 yr B.P. at Effingham Inlet; R. Enkin, 2009, personal commun.). However, one of these debris flows may correlate instead with a probable crustal earthquake at ~2000 yr B.P. that caused subsidence near Victoria and Vancouver (Fig. 1; Mathewes and Clague, 1994), at sites where no discernable megathrust coseismic displacements are expected.

Event Comparison

Table 1 provides a summary of coseismic subsidence estimates at each Cascadia marsh (see Fig. 3 for locations) both for the A.D. 1700 event and, where available, pre–A.D. 1700 events (detailed compilation is available in Table DR1 [see footnote 1] and Fig. 5). At each site, the mean subsidence (weighted by higher-quality data where possible), standard deviation, and mean uncertainty are given, as well as the number of buried soils represented. Higher-quality estimates are marked in Table 1 and shown with darker symbols in Figure 5.

The pre–A.D. 1700 mean subsidence may be biased toward larger events. Some relatively small turbidites have few or no correlatives in the marsh record despite the inference of shaking for significant distances along strike (Goldfinger et al., 2008). These turbidites may represent smaller earthquakes with restricted rupture length and/or a short preceding strain accumulation period. Some buried soils may also be missed; for example, at Willapa Bay (Redtail locality), no visible horizon was found between those soils correlated with events T1 and T4, yet an analysis of diatoms showed an intervening sharp transition from a high marsh to probable tidal flat environment (Atwater and Hemphill-Haley, 1997). If two or more earthquakes occur very close together in time, there is also the chance of under-representation in the turbidite record and/or misinterpretation of it; one turbidite may cause erosion of a previous deposit, or there may be a lack of intervening pelagic sediment. For example, Goldfinger et al. (2003) reported 18 marginwide events in the Holocene, but one "event" was later recognized as a couplet representing two events, thus making it 19 (e.g., Goldfinger et al., 2008).

We use the mean pre–A.D. 1700 coseismic displacements to characterize an average Cascadia event (pre–A.D. 1700 mean in Fig. 6; Table 1). Mean coseismic subsidence is 1.0–1.6 m in southern Washington, 0.4–0.9 m in the northern half of Oregon, 0.7–1.2 m in the southern half of Oregon, and 0.7–0.95 m in northern California. At the northern end of the margin, with only one qualitative pre–A.D. 1700 data point (at Deserted Lake, Vancouver Island), we cannot define the subsidence for an average event. On this basis, events T4, T5, T6, and T9 appear most similar to an average long-rupture Cascadia earthquake (Figs. 5 and 6). Of the other full- or nearly full-rupture events, the least similar to the average are events T2 and 5a, which show low to absent coseismic displacements in N. Oregon/S. Washington (~46–47°N), but close to mean displacements in central and southern Oregon and northern California.

Within the data uncertainties (~±0.5 m), the subsidence produced by the A.D. 1700 earthquake was similar to that produced by an average pre–A.D. 1700 Cascadia megathrust earthquake (Fig. 6; Table 1). Subsidence in A.D. 1700 in southern Washington and northern Oregon was greater than average by up to 0.6 m (except at Netarts Bay), although the difference is at the limit of the data resolution. At the northern end of the margin (Vancouver Island), microfossil data at Deserted Lake (showing a sudden and lasting change to more saline conditions) imply less coseismic subsidence in the A.D. 1700 earthquake (<0.5 m) than during event T5 (Hutchinson et al., 2000). Unfortunately, there are no other data from earlier events at this or other Vancouver Island sites for further comparison.

ELASTIC DISLOCATION MODELING

Coseismic Models

We compared observations of coastal subsidence compiled here with predictions of vertical coseismic displacement based on the CAS3D elastic dislocation model (Wang et al., 2003). We assumed a shallow full-rupture zone, where strain accumulated by plate convergence is released seismically in great earthquakes, and a transition zone with a linear decrease from full seismic rupture updip to zero seismic rupture downdip (Fig. 3). Although some models suggest partial interseismic strain accumulation on the shallow fault zone (e.g., McCaffrey et al., 2007), we assume that the seismogenic portion of the fault is fully locked, and that coseismic rupture releases the full strain accumulated at plate convergence rates during the interseismic period. It remains uncertain whether megathrust earthquakes fully release the strain accumulated over one earthquake cycle, or if coseismic slip summed over many earthquake cycles releases the total strain accumulated over that time (Wang, 2007). We assume a convergence rate between the Juan de Fuca and North America plates that increases northward from 26 mm/yr toward 039° in the south to 45 mm/yr toward 056° in the north, consistent with plate models (e.g., Mazzotti et al., 2003; McCaffrey et al., 2007). Our model does not account for the small effect of the motion of the Cascadia forearc relative to North America (e.g., Wells and Simpson, 2001; McCaffrey et al., 2007).

Full coseismic strain release is assumed to occur within the interseismic locked zone (Fig. 3), with updip and downdip extents consistent with geodetic data (e.g., Wang et al., 2003), thermal constraints (e.g., Hyndman and Wang, 1993), and inferences from the A.D. 1700 tsunami recorded in Japan (e.g., Satake et al., 2003). There is much uncertainty on the coseismic rupture behavior at the updip end of the fault, e.g., slip may transfer onto steep splay faults (e.g., Flück et al., 1997). The models of Wang and He (2008) show that megathrust ruptures are generally not expected to break the seafloor at the trench; such blind fault behavior results in greater seafloor uplift than trench-breaking ruptures. The updip rupture behavior is thus crucial for tsunami generation, but it has very little impact on vertical displacements at the coast.

Recent interseismic dislocation models such as CAS3D include a wide time-dependent ("effective") downdip transition zone to incorporate viscoelastic effects through the earthquake cycle (e.g., Wang et al., 2003). The effective transition zone partially simulates postseismic stress relaxation, and its width increases with time in the earthquake cycle, so it is appropriate to use a narrower transition zone for the coseismic model (e.g., Satake et al., 2003). The coseismic transition zone used here corresponds to the seaward half of the effective transition zone of Wang et al. (2003), and it is the same as the transition zone used in the "Long-Narrow" model of Satake et al. (2003).

Coseismic Deformation for Given Return Intervals

We modeled the coseismic release of strain accumulated over time periods of 200–500 yr (encompassing the range of estimated recurrence intervals) to predict coastal displacements (Figs. 5, 6, and 7B). Figures 6B and 7B show coseismic vertical displacements modeled at the coastal marsh locations for full-margin ruptures. Along-strike variations in these displacements are primarily due to variations in the location of marsh sites (on a margin-normal profile) with respect to the full-rupture and transition zones (Figs. 2, 7A, and

TABLE 1. MEAN SUBSIDENCE AND SLIP IN A.D. 1700 (T1) AND PRE–1700 CASCADIA EVENTS ESTIMATED AT COASTAL SITES

Location	Mean latitude (°N)	Mean longitude (°W)	Soils*	Subsidence mean†,σ§,mean uncert.# (m)	Slip** mean†,σ§,mean uncert.# (m)	Data sources††
Deserted Lake	49.762	126.507	1700	Small; <~0.5 m	?	1
			pre–1700(1)	>T1	>T1	1
Port Alberni	49.254	124.825	1700	0.10,0.13,0.50	6,8,31	2
Tofino	49.106	125.846	1700§§	0.61,0.09,0.33	6,1,3	3–6
Copalis R.	47.121	124.162	1700	1.37,0.38,0.57	27,8,11	8,9
			pre–1700(2)	1.25,0.64,0.50	25,13,10	8,9
Grays Harbor_E	46.953	123.737	1700	1.76,0.19,0.40	34,3,8	8,10,11
			pre–1700(4)	1.19,0.73,0.45	24,15,9	8
Grays Harbor_W	46.913	124.006	1700§§	1.12,0.60,0.4	20,10,7	11,12
			pre–1700(8)§§	1.04,0.57,0.46	18,10,8	8,12
Willapa Bay_E	46.672	123.734	1700	1.20,–,0.50	31,–,13	8
			pre–1700(7)	1.00,0.22,0.67	26,13,17	8
Willapa Bay_W	46.570	123.935	1700§§	1.51,0.51,0.70	29,10,14	7,8,13–16
			pre–1700(6)§§	1.56,0.41,0.92	30,8,18	8,13,14,16
Columbia R._E	46.244	123.437	1700	0.80,0.30,0.60	(68,23,51?)	10,17
Columbia R._W	46.262	123.701	1700	1.72,0.22,0.51	(76,28,22?)	8,10,18,19
			pre–1700(3)	1.71,0.08,0.53	(73,4,23?)	8,16
Necanicum R.	45.985	123.917	1700	0.64,0.40,0.50	18,12,14	10,11,20–22
			pre–1700(3)	0.35,0.52,0.50	10,15,14	8,16
Nehalem R.	45.699	123.881	1700§§	0.66,–,0.31	27,–,13	23
Tillamook Bay	45.521	123.902	1700	1.44,0.26,0.40	64,13,18	10,11
			pre–1700(1)	0.85,–,0.40	35,–,17	11
Netarts Bay	45.387	123.953	1700§§	0.55,0.21,0.48	23,10,21	24
			pre–1700(7)	0.83,0.38,0.44	34,15,18	20,21,24,25
Nestucca Bay	45.178	123.936	1700	0.88,0.23,0.45	44,11,22	10,20,21,23
			pre–1700(14)	0.67,0.16,0.49	34,8,25	21
Salmon R.	45.033	123.994	1700§§	0.77,0.19,0.39	37,10,19	10,23,26
			pre–1700(4)§§	0.35,0.11,0.33	17,5,15	26
Siletz Bay	44.901	124.016	1700	0.62,0.18,0.40	30,9,19	10,11,20,21,27
			pre–1700(7)	0.50,0.27,0.39	25,14,19	10,21,27
Yaquina Bay	44.593	123.963	1700	0.41,0.24,0.43	22,15,23	10,20,21,28
			pre–1700(10)	0.56,0.14,0.39	40,10,28	21
Alsea Bay	44.420	124.018	1700§§	0.40,–,0.20	20,–,10	29
			pre–1700(10)	0.44,0.12,0.35	22,6,18	29,30
Siuslaw R.	43.987	124.016	pre–1700(3)	0.75,0.23,0.51	39,14,19	31,32
Umpqua R.	43.690	124.071	1700	0.53,0.03,0.46	20,2,17	31,32
			pre–1700(10)	0.72,0.34,0.51	30,15,21	10,31
Coos Bay_E	43.440	124.190	1700	0.60,0.17,0.43	14,4,10	32
			pre–1700(8)	0.69,0.12,0.52	16,3,12	31,32
Coos Bay_W	43.299	124.322	1700§§	0.80,0.14,0.34	12,2,5	23,32,35
			pre–1700(12)§§	0.81,0.15,0.62	11,2,9	31,22,33–35
Coquille R.	43.146	124.373	1700	0.77,0.30,0.58	9,3,7	10,32,37–39
			pre–1700(11)§§	1.19,0.42,0.91	15,5,12	36
Sixes R.	42.831	124.535	1700§§	1.50,–,1.10	19,–,14	40
			pre–1700(11)§§	0.99,0.36,0.78	12,4,10	41
Humboldt Bay_E	40.855	124.128	1700§§	0.86,0.12,0.65	10,1,8	10,42–46
			pre–1700(10)	0.74,0.14,0.58	10,2,8	44–46
Humboldt Bay_W	40.680	124.216	1700	0.80,0.00,0.60	38,3,28	46,47
			pre–1700(8)	0.66,0.15,0.50	28,6,21	10,46,47
Eel R.	40.619	124.315	pre–1700(4)	0.95,0.06,0.68	(–44,33,31?)	48
Singley Flat	40.427	124.403	1700	Uplift, not quantified	?	49,50

*A.D. 1700 soil, or mean of pre–1700 soils; number of pre–1700 soils in parentheses.
†Mean weighted by data quality for individual events where possible.
§Standard deviation of estimates. Where none is given (–), there is only one estimate.
#Mean uncertainty of individual estimates.
**Model slip that best fits subsidence estimates; uncertainties are propagated from subsidence estimate uncertainties.
††Sources of sedimentological and/or subsidence data: 1—Hutchinson et al. (2000), 2—Clague and Bobrowsky (1994a), 3—Guilbault et al. (1996), 4—Clague and Bobrowsky (1994b), 5—Guilbault et al. (1995), 6—Hughes et al. (2002), 7—Peterson et al. (2000), 8—Atwater (1988), 9—Atwater (1992), 10—Peterson et al. (1997), 11—Barnett (1997), 12—Shennan et al. (1996), 13—Sabean (2004), 14—Atwater and Hemphill-Haley (1997), 15—Hemphill-Haley (1995), 16—Atwater et al. (2004a), 17—Atwater (1994), 18—Peterson and Madin (1997), 19—Peterson et al. (1993), 20—Darienzo (1991), 21—Darienzo et al. (1994), 22—Darienzo and Peterson (1995), 23—Hawkes et al. (2008), 24—Shennan et al. (1998), 25—Darienzo and Peterson (1990), 26—Nelson et al. (2004), 27—Peterson et al. (1996), 28—Peterson and Priest (1995), 29—Nelson et al. (2008), 30—Peterson and Darienzo (1991), 31—Briggs (1994), 32—Nelson (1992a), 33—Peterson and Darienzo (1989), 34—Nelson et al. (1998), 35—Nelson et al. (1996), 36—Witter et al. (2003), 37—Witter et al. (1997), 38—Nelson (1992b), 39—Briggs and Peterson (1993), 40—Kelsey et al. (1998), 41—Kelsey et al. (2002), 42—Carver and Burke (1989), 43—Jacoby et al. (1995), 44—Pritchard (2004), 45—Vick (1988), 46—Valentine (1992), 47—Patton and Witter (2006), 48—Li (1992), 49—Carver et al. (1994), 50—Merritts (1996).
§§Values represent high-quality subsidence estimates, from detailed microfossil analyses.

7B). Variations in displacement are also associated with along-margin changes in both the plate convergence vector and the width of the full-rupture zone (Fig. 6A).

For the central part of the margin (Oregon and southern Washington), the marsh data are broadly consistent with the pattern of coseismic displacements predicted for the full release of strain accumulated over 500 yr (Figs. 5 and 6B), although some departures from this pattern are suggested. In particular, in Washington and northernmost Oregon, the data suggest greater coseismic slip and, by inference, a longer period of strain accumulation, especially for the A.D. 1700 event. At the northern end of the margin (Vancouver Island), the paleoseismic subsidence data for the A.D. 1700 earthquake point to a relatively short strain accumulation time

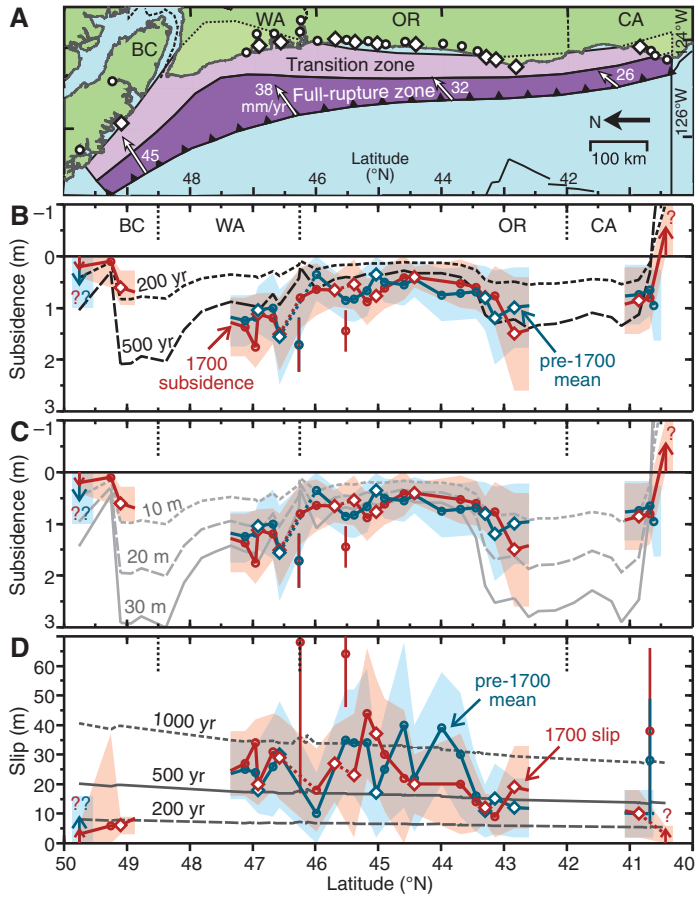

Figure 6. Comparison of coseismic subsidence and megathrust slip among the A.D. 1700 earthquake (T1), previous recorded events (averaged), and the predictions of elastic dislocation models. Subsidence and slip estimate details are given in Table 1 (with all subsidence data in Table DR1 [see footnote 1]). (A) Averaged locations of coastal coseismic subsidence sites relative to the full-rupture (purple) and transition (lilac) zones. White diamonds and circles—sites with high- and low-quality subsidence estimates, respectively. See Figure 3 for site names. White arrows—plate convergence vectors. (B) Coseismic subsidence estimated at the above buried soil sites for the A.D. 1700 earthquake (red symbols and shading—weighted mean and uncertainty) and for pre–A.D. 1700 recorded events (blue symbols and shading—mean and uncertainty). Upward/downward arrows with question marks indicate unquantifiable estimates of uplift/subsidence. Two low-quality data points are excluded from the shading as they appear to be outliers; these include data from the Columbia River that are questionable due to possible freshwater influence (Leonard et al., 2004). Dashed dark-gray lines show coseismic subsidence predicted by the elastic dislocation model at the same sites for the release of 200 and 500 yr of accumulated strain. (C) As in B, except the gray lines represent coseismic subsidence predicted for uniform megathrust slip of 10, 20, and 30 m. (D) Along-strike megathrust slip variations estimated for the A.D. 1700 (red symbols and shading—weighted mean and uncertainty) and previous events (blue symbols and shading—mean and uncertainty) from the correspondence between observed coseismic subsidence and that predicted from uniform slip models (C). Dark-gray lines show the along-margin slip pattern expected for the release of 200, 500, and 1000 yr of accumulated strain.

(~200 yr). In the south (northern California), the higher-quality coseismic subsidence data from Humboldt Bay also imply accumulation times of less than 500 yr. Coseismic uplift at Singley Flat is not quantified, and the marsh data from Eel River, which lies between Humboldt Bay and Singley Flat (Fig. 3), show coseismic subsidence instead of the uplift predicted by modeling. Thus, the data suggest that the zero isobase (marking the transition from uplift near the deformation front to subsidence inland) occurs on the seaward (west) side of Eel River rather than on its landward side as predicted by the model. In a later section, we examine variations in the dislocation model that may resolve these discrepancies.

Estimated Megathrust Slip

In addition to the strain release models described, we estimated approximate coseismic slip on the megathrust for both average (Fig. 6D; Table 1) and individual events (Fig. 8) by finding the best fit to the data at each site. The comparison in Figure 8 shows that, given the large uncertainties, the events show generally similar along-margin slip patterns. For most events, slip magnitudes tend to be highest on the central part of the margin (~44–45.5°N), with mean slip of 28 ± 9 m. Lower mean slip of 24 ± 6 m and 15 ± 6 m occur in the north-central (~46–47°N) and south-central (~42.5–44°N) regions, respectively (Table 1).

The A.D. 1700 earthquake (T1) shows mean slip magnitudes for the central margin that are similar to previous events, but somewhat larger in southern Washington and northernmost Oregon (Fig. 6D; Table 1). In the event prior to A.D. 1700 (T2; Figs. 5 and 8), subsidence, and, consequently, megathrust slip appear to be very small in this region, and thus it is possible that this part of the fault "caught up" on the slip deficit with above-average displacements in A.D. 1700 (although there may also be a postseismic deformation effect; see following). A similar phenomenon occurred in the 1960 Chile megathrust event, in which coseismic deformation was significantly greater than expected from the preceding interval, and the previous event released less strain than expected (Cisternas et al., 2005).

For the northern and southern ends of the margin, only limited data are available for pre–A.D. 1700 events. In the north (Deserted Lake), the subsidence data are qualitative and we can only say that megathrust slip was less in A.D. 1700 than in event T5. In the south, slip estimates are complicated by a misfit in the zero isobase between the model and the data. The model predicts uplift at Eel River, and significantly lower subsidence in western than eastern Humboldt Bay, neither of which agree with the marsh data, resulting in negative slip estimates at Eel River, and vastly different slip estimates (by 20–30 m) for similar amounts of subsidence at western and eastern Humboldt Bay (Table 1). However, from the subsidence data, we infer that megathrust slip in the A.D. 1700 event was similar to previous events in this region.

Variations in Earthquake Rupture Downdip Width

Model predictions of coseismic displacement are dependent on the magnitude of megathrust slip, as outlined above, but also on the width of the coseismic rupture zone, especially the downdip extent. Variations in the updip limit have a negligible effect on coastal displacement, as noted previously. In the models, we used the

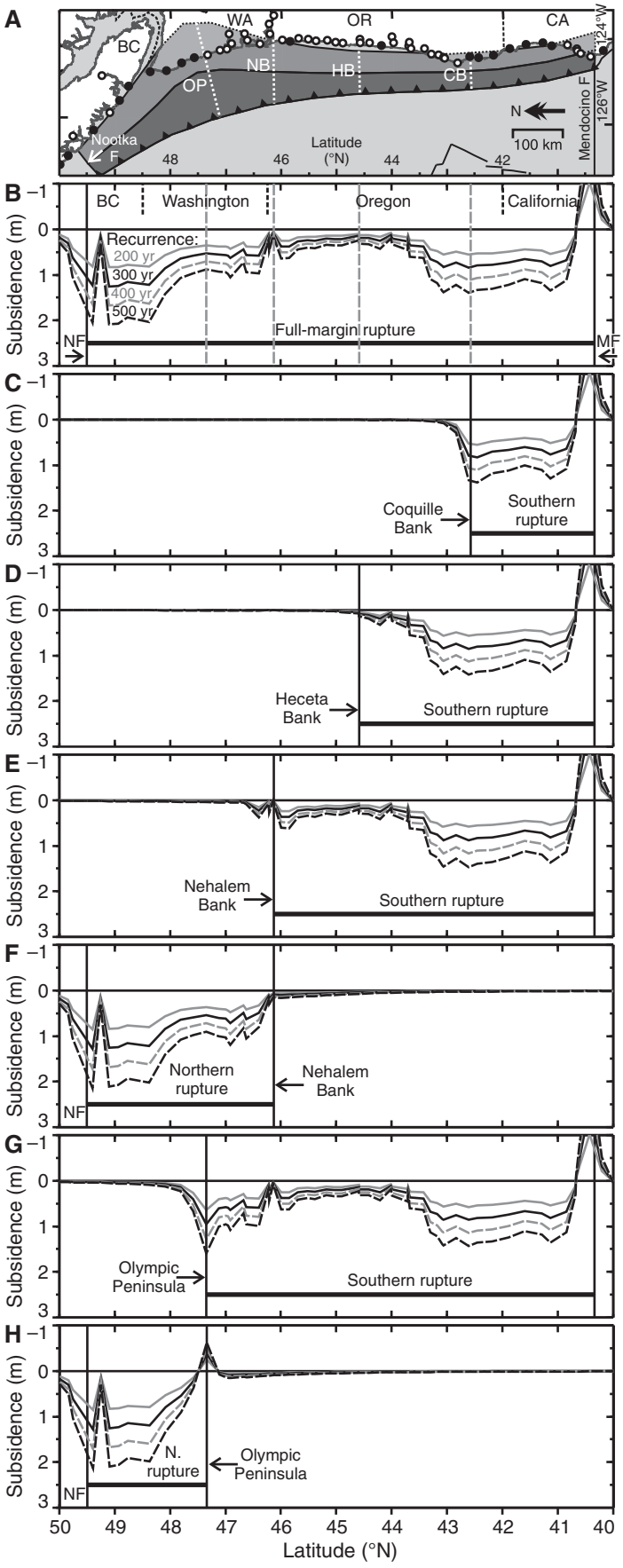

Figure 7. Patterns of coseismic subsidence along the Cascadia coast predicted by modeling the release of 200, 300, 400, and 500 yr of strain accumulated at current plate rates for various rupture modes. (A) Site locations where subsidence was predicted: sites with coseismic subsidence data for past events (white-filled circles); intervening sites with no data (black circles). (B) Full-margin rupture from the Mendocino fault (MF) in the south to the Nootka fault (NF) in the north. (C, D, E, G) Rupture from Mendocino fault (MF) north to Coquille Bank (CB), Heceta Bank (HB), Nehalem Bank (NB), and the Olympic Peninsula (OP), respectively. (F, H) Rupture from Nootka fault (NF) south to Nehalem Bank, and Olympic Peninsula, respectively. Southern ruptures to segment boundaries Coquille Bank, Heceta Bank, and Nehalem Bank were proposed by Goldfinger et al. (2008) as matching rupture extents from paleoseismic data. These boundaries approximately coincide with apparent boundaries in events of episodic tremor and slip (Brudzinski and Allen, 2007). We also investigate northern ruptures to Nehalem Bank, and to Olympic Peninsula, an additional episodic tremor and slip boundary that has no apparent megathrust paleoseismic record.

Figure 8. Approximate megathrust slip in events 1–9 (T1–T9), as correlated in Figure 4, plotted against latitude. Slip is estimated by calculating the magnitude of modeled slip that corresponds to the subsidence estimates (and uncertainties) at each location. Excluded are data from Eel River, for which negative slip values were calculated (Table 1) due to misfit between observed and modeled subsidence. Symbol style represents quality of original subsidence estimates as in Figure 5. Thick black lines and gray shading represent the weighted average (moving average over 1°) and uncertainty, respectively, of calculated megathrust slip. Thinner gray lines, labeled for event 2, show the model slip deficit along the margin for 200, 500, and 1000 yr, corresponding to slip rates that increase northward from 26 to 45 mm/yr due to along-margin changes in the plate convergence vector.

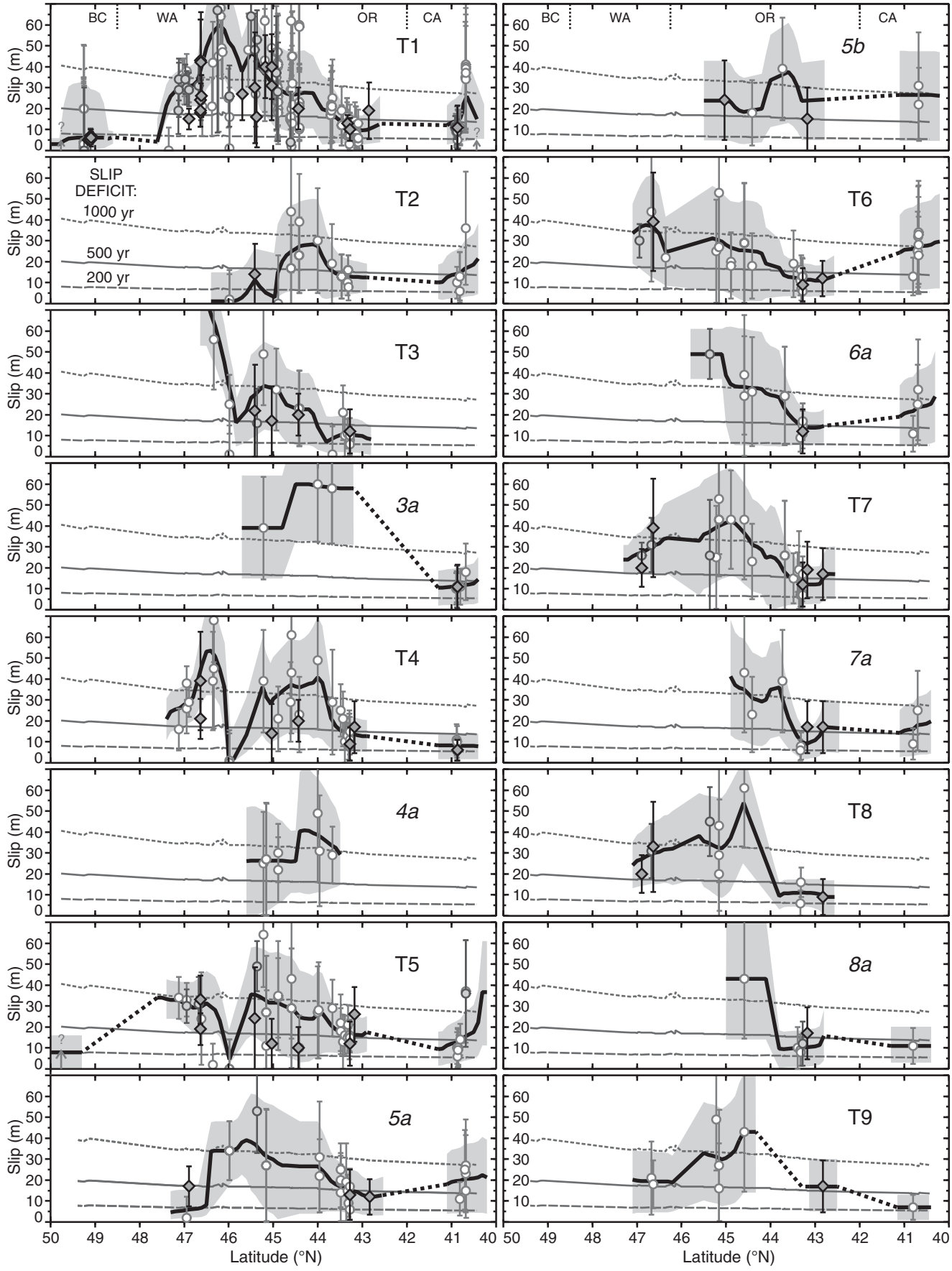

interseismic locked zone as determined from geodetic and thermal data as the region of full coseismic rupture (Fig. 3) and found general agreement with the constraints from the coastal data. We now examine the effect of variations in the downdip limit such that the total width of the full-rupture zone varies by ±25%, consistent with uncertainties in the definition of the thermal and geodetic interseismic locked zone (e.g., Hyndman and Wang, 1995; McCaffrey et al., 2000; Mazzotti et al., 2003). We do not vary the downdip limit of the transition zone; such variations have little effect on surface deformation due to the small amount of slip in the deep transition zone.

For most of the coast, there are subsidence data only at one distance landward of the trench (Fig. 3), but in several areas there are limited data for subsidence variations with distance on a trench-perpendicular profile, allowing assessment of variations in rupture zone width (Fig. 9). Variations in rupture width affect the modeled coseismic vertical displacement in two ways. First, the zero isobase approximately coincides with the downdip limit of full rupture; a wider rupture zone shifts this point landward. Secondly, an increase in rupture width increases the maximum magnitude of vertical deformation. At most sites, the marsh data lie landward of the zero isobase of all models, and thus only the magnitudes of modeled coastal subsidence can be compared with the marsh data. A variation of 25% in the rupture width changes the modeled displacements by less than 0.5 m at most sites, well within the uncertainties of the marsh data, which are therefore of limited use in constraining the rupture zone width. The data scatter highlights the need for more high-precision microfossil studies of coseismic displacement in order to improve the constraints. Discrepancies between the marsh observations and the dislocation model predictions can be resolved by varying the amount of fault slip (dashed lines show best-fit slip in Fig. 9), i.e., there is a trade-off between slip magnitude and rupture width.

Better constraints on rupture width can be provided by coseismic data that lie near the zero isobase. This location lies offshore along most of the Cascadia margin, except in the south (northern California; Fig. 3). Here, marsh data for the A.D. 1700 (Singley Flat and Humboldt Bay) and previous events (Eel River and Humboldt Bay) indicate approximately similar coseismic subsidence at Eel River and Humboldt Bay, with uplift (of nonquantified magnitude) at Singley Flat, ~10 km further west (Fig. 9D). However, the model predicts uplift at both Eel River and Singley Flat, and a steep decline in displacement values from eastern to western

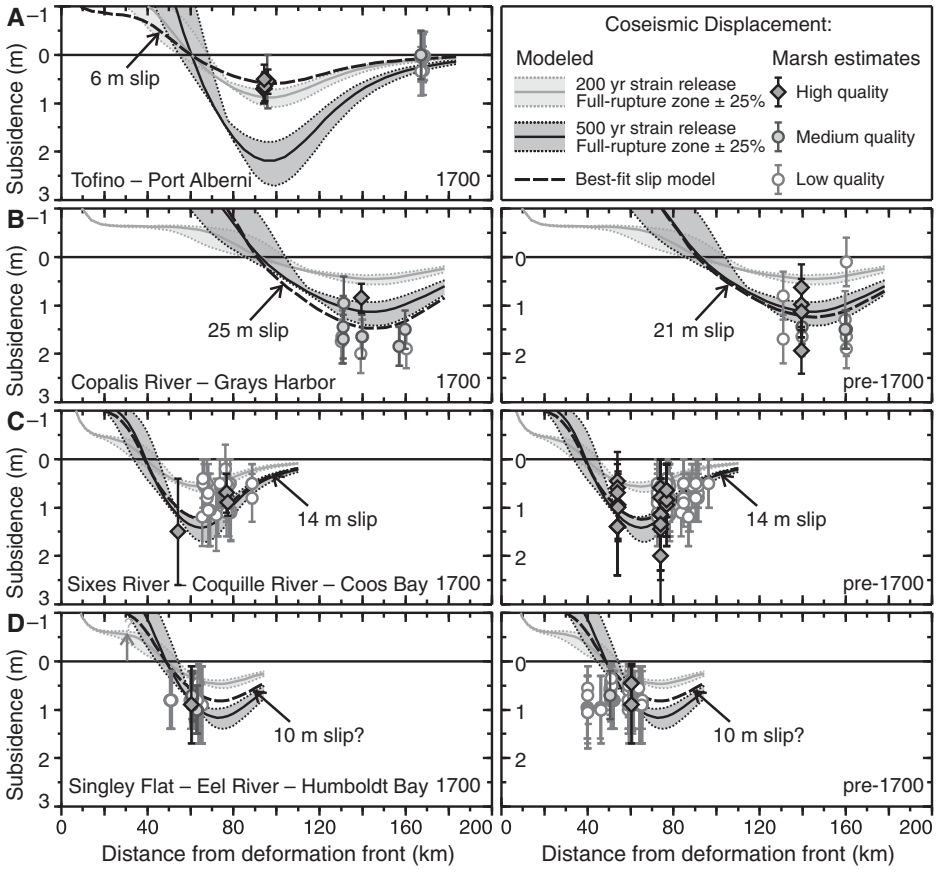

Figure 9. Effect of variations in the rupture width on the modeled coseismic surface vertical motion for four profiles oriented perpendicular to the margin (see Fig. 3 for locations A–D). Rupture width is varied by ±25% by changing the position of the downdip limit of rupture, relative to the reference downdip limit. The amount of slip is equal to the amount of strain accumulated over 200 yr (solid gray lines and light-gray shading for full-rupture zone width ±25%) and 500 yr (solid black lines and darker gray shading) at plate convergence rates. Marsh subsidence data (with uncertainties) within a 40–80-km-wide swath centered on the profile lines are shown for the A.D. 1700 event (left) and previous events (right). Dashed black lines show the megathrust slip (reference rupture zone width) that best fits the weighted mean of the data. Question marks in D convey uncertainty in megathrust slip estimate due to data-model misfit.

Humboldt Bay that is not apparent in the marsh data. Due to this misfit, estimation of megathrust slip is meaningless here (Table 1). The misfit in southern Cascadia may relate to the proximity of the Mendocino triple junction and the breakup of the Gorda plate (e.g., Wang and Rogers, 1994; Chaytor et al., 2004; Fig. 1). The elastic dislocation model for megathrust earthquake rupture is not designed to account for the complex crustal deformation within ~100 km of a triple junction (Wang et al., 2003; Wang, 2007). The more westward transition from uplift to subsidence indicated by the marsh data could be better fit by a model with a rupture zone that is narrower (by ~25%) than the reference locked zone in this region (Fig. 9D).

Variations in Rupture Length—Segmented Ruptures

An important question for seismic hazard characterization concerns the along-margin rupture extent: Can we expect the megathrust fault to always rupture in one large (M ~9) earthquake along the whole margin, or does it sometimes rupture in a series of smaller events (M ~8) on adjoining segments? Historical tsunami records from Japan (e.g., Satake et al., 2003), tsunami run-up documented at the Cascadia coast (e.g., Clague et al., 2000; Peters et al., 2003), and the turbidite record (Goldfinger et al., 2003), show that the A.D. 1700 earthquake must have ruptured almost the entire margin in a single M ~9

earthquake. As mentioned previously, the onshore paleoseismic record for earlier events is lacking in temporal resolution, but the turbidite record provides evidence for large-scale local and synchronous shaking, allowing for better discrimination between full-margin and shorter ruptures. Goldfinger et al. (2008) found that southern margin ruptures of various length are almost as common (45%) in the Holocene record as full or nearly full-length ruptures (50%). 5% of ruptures cover only the central and southern margin, but there is no evidence for short ruptures in the northern region.

Goldfinger et al. (2008) proposed that segment boundaries occur at forearc structural highs in southern (Coquille Bank), central (Heceta Bank), and northernmost Oregon (Nehalem Bank) (Fig. 7A). They noted an approximate coincidence of these limits with apparent boundaries between zones of differing episodic tremor and slip recurrence (Brudzinski and Allen, 2007). An additional episodic tremor and slip boundary at the Olympic Peninsula (Fig. 7A; Brudzinski and Allen, 2007) does not appear to have a paleoseismic equivalent. We investigate segmented ruptures by modeling the predicted coseismic displacement at coastal sites (Fig. 7A) for 200–500 yr of accumulated slip for the various rupture modes proposed by Goldfinger et al. (2008) from the turbidite record (Figs. 7B–7E), as well as for hypothetical ruptures in the south (extending as far north as the Olympic Peninsula; Fig. 7G) and the north (from the Nootka fault to Nehalem Bank and the Olympic Peninsula; Figs. 7F and 7H).

It is difficult to differentiate between full-margin events and those rupturing only as far north as the Olympic peninsula because onshore coseismic displacement data for pre–A.D. 1700 events are almost completely lacking north of southern Washington (Fig. 5), tsunami deposits cannot be used to discriminate rupture origin, and both rupture modes could potentially generate turbidity currents as far north as the head of Juan de Fuca canyon (~48°N). However, northern segment ruptures should produce additional turbidites at Juan de Fuca canyon and possibly Cascadia channel (see Goldfinger et al., 2008, 2010), but none has been recognized. The expected magnitude for a megathrust earthquake along the northern 100–280 km of the subduction zone is M_w = 8.0–8.6 (assuming a rupture width of 70–95 km and 5–10 m of coseismic slip; Fig. 10). It is unlikely that there has been an undetected M >8 earthquake in the last 200–300 yr (historical time), or indeed one that escaped the turbidite record throughout the Holocene. Preliminary results of ongoing work on paleoseismic records from southern Vancouver Island (Saanich and Effingham Inlets) do not suggest independent northern megathrust events (Blais-Stevens et al., 2009; R. Enkin, 2009, personal commun.). Goldfinger et al. (2007b) proposed that the lack of Holocene segmentation for northern Cascadia is related to the large thickness (3–4 km) of submarine sediments that likely smooth the plate interface and promote through-going rupture. Sediment thickness tapers southward along the margin, which may allow forearc structures to play a greater role in controlling rupture extent in southern Cascadia.

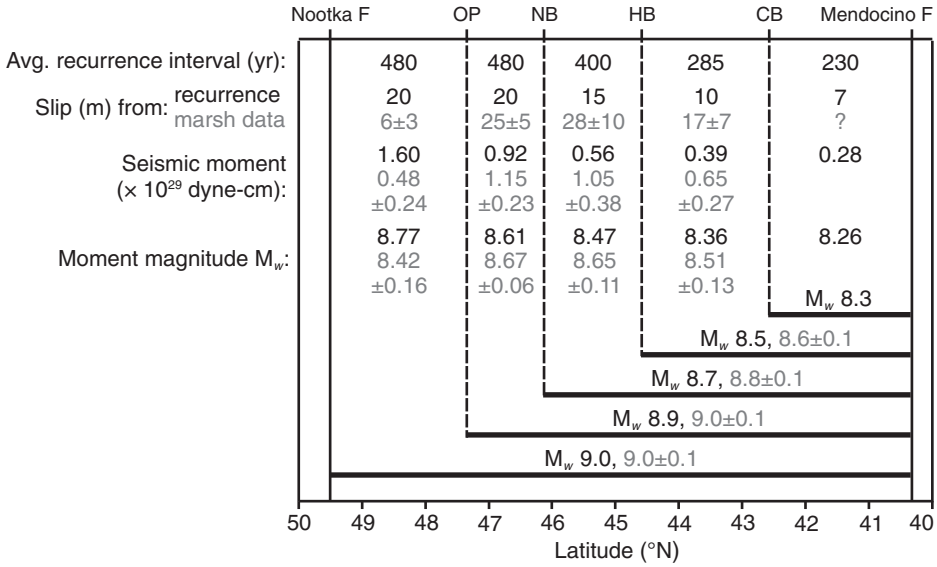

Figure 10. Moment magnitude values estimated for full-margin and segmented ruptures of the Cascadia megathrust. Seismic moment is estimated using the equation $M_o = \mu A s$ (Hanks and Kanamori, 1979), where μ, the shear modulus, is taken to be 3.0×10^{11} dyne-cm (a typical value for crustal rocks; Turcotte and Schubert, 2002), *A* is the rupture area, and *s* is the magnitude of slip. Rupture widths are approximated downdip by the width of the full-rupture zone and half the width of the transition zone, and rupture lengths are measured between the Nootka and Mendocino faults and the various segment boundaries shown in Figure 7. Slip values are approximated for each segment of the margin, (1) from the expected slip related to average recurrence intervals over the past 6500 yr (black text), and (2) from the best fit to the average marsh displacements (gray text). The expected moment contribution of each segment is given for both slip approximations, along with moment magnitudes, calculated using the equation $M_w = 2/3 \log(M_o) - 10.7$ (Hanks and Kanamori, 1979). Moment magnitudes are also given for various rupture modes shown in Figure 7. Marsh data for the northernmost segment are based only on the A.D. 1700 event; a preceding interval of ~200 yr is expected to lead to an earthquake with 8 m slip, 0.64×10^{29} dyne-cm moment release, and M_w 8.50. Abbreviations: Coquille Bank (CB), Heceta Bank (HB), Nehalem Bank (NB), and the Olympic Peninsula (OP).

For all segmented ruptures (Figs. 7C–7H), modeled coseismic vertical displacements are identical to a full-margin rupture (Fig. 7B) for the region of the rupture zone itself, except within ~50 km of the rupture edge, where displacements either taper rapidly to zero or show abrupt variations likely due to artificial model edge effects (e.g., Olympic Peninsula). Beyond the edge of rupture, coseismic displacements decrease rapidly to near-zero within 50 km. Thus, if coseismic displacements are sufficient to leave a marsh paleoseismic signature, the site must lie either within the margin-parallel extent of the rupture zone or no further than ~50 km beyond it. The along-margin rupture extent of individual events inferred from the onshore buried soil record (where data exist) should therefore be approximately consistent with those deduced from the turbidite record of Goldfinger et al. (2008, 2010).

In Figure 10, we calculate the expected seismic moment release and moment magnitude of seismic ruptures on each subduction zone segment, and of multiple-segment ruptures. Megathrust slip is approximated in two ways: (1) by the strain accumulated over the average recurrence interval for each segment, and (2) from the best fit to the average marsh displacements. Seismic moment release compatible with marsh data is somewhat greater for the central segments, and significantly less for the northernmost

segment, than expected from average recurrence intervals. The marsh data in the north are based only on the last megathrust event, and they are consistent with the preceding interval of ~200 yr. Earthquake magnitudes for the different rupture modes proposed by Goldfinger et al. (2008) range from M_w 8.3–8.8 for the southern ruptures (rupture modes from Figs. 7C–7E) to M_w 9.0 for a full-margin event (Fig. 10).

Transient Fault and Mantle Behavior

Small (up to 30 cm) land-level changes occurring gradually over several years prior to megathrust earthquakes have been detected in microfossil studies in Cascadia and Alaska (e.g., Hawkes et al., 2005; Shennan and Hamilton, 2006). Such preseismic motions, for which the cause is yet to be established, should not contaminate the coseismic subsidence estimates, as long as the uppermost part of the buried soil is sampled. A more significant factor may be the inclusion of some postseismic deformation. Several studies suggest that coastal marsh elevation indicators are reestablished within a few weeks of an earthquake (e.g., Ovenshine and Kachadoorian, 1976; Hemphill-Haley, 1995), but this time interval is not well constrained. Thus, along with the coseismic signal, it is possible that the elevation differences recorded in marshes may also include slow vertical ground motion associated with postseismic transients over days to months following a great earthquake.

One key transient signal may come from aseismic slip along the megathrust interface (commonly called afterslip) over days to years after an earthquake (e.g., Melbourne et al., 2002; Zweck et al., 2002). Global positioning system (GPS) observations following the 1995 Jalisco Mexico (Hutton et al., 2001; Melbourne et al., 2002), 2004 Sumatra-Andaman (e.g., Chlieh et al., 2007; Paul et al., 2007; Gahalaut et al., 2008), and 2005 Nias-Sunda earthquakes (Hsu et al., 2006) show that the postseismic signal can be modeled by afterslip on the deep part of the megathrust fault below the coseismic rupture area. Another transient signal comes from viscous relaxation of the large stresses induced by a great earthquake in the material surrounding the rupture zone. Although relaxation is thought to be most important on time scales of decades to centuries, it may explain short-term surface deformation following great earthquakes in SW Japan, Chile, and Alaska (e.g., Wang, 2007).

Complex time-dependent models that include both elastic and viscous behavior are required to properly address postseismic slip and viscous relaxation following a great earthquake. Such models are beyond the scope of the current study. Instead, we present an elastic dislocation model that approximates the integrated effects of shallow coseismic and deep postseismic slip to assess the ways in which coastal subsidence estimates may be affected, using the Vancouver Island and central Washington profiles as examples. During the coseismic phase, slip corresponding to 200 or 500 yr of strain accumulation is assumed on the full-rupture zone (as modeled previously). The postseismic phase is modeled by slip on the deeper part of the fault. Both afterslip and viscous relaxation appear to occur primarily below the coseismic rupture zone, but the maximum depth is not well constrained (e.g., Gahalaut et al., 2008). Our simplified model has a "postseismic slip zone" that extends from the downdip limit of the full-rupture zone to the halfway point of the transition zone. The magnitude of postseismic slip is also poorly constrained, and most observations suggest that it varies over time (e.g., Hutton et al., 2001; Wang, 2007; Gahalaut et al., 2008). We assign a uniform along-margin slip of 5 m, similar to the inferred afterslip over 6 mo following the Sumatra-Andaman earthquake (Chlieh et al., 2007; Gahalaut et al., 2008). The "postseismic slip zone" is bounded on either end by transition zones, where slip decreases linearly from 5 m to zero; the updip transition zone extends to the deformation front, and the downdip transition zone extends to the deep limit of the coseismic transition zone.

Figure 11 shows the modeled coseismic and postseismic vertical deformation along the two profiles, in comparison with marsh data for the A.D. 1700 and previous events. Due to the greater depth of the postseismic slip, the zero isobase is shifted 20–30 km landward of the coseismic zero isobase. The total vertical displacement after both phases of slip (solid line in Fig. 11) can be divided into three regions. Far inland from and close to the deformation front, the postseismic slip produces vertical motion of the same sign as the coseismic slip, thus enhancing the total subsidence and uplift, respectively. The intervening area will first subside during coseismic rupture, and then uplift during postseismic slip. Here, the net subsidence/uplift budget will depend on the ratio and spatial distribution of coseismic to postseismic slip.

In these examples, if marsh elevation indicators are not established within days in postearthquake sediments, early postseismic slip could result in coseismic subsidence being overestimated at the coastal sites. A similar situation applies to most Cascadia marshes, but coseismic subsidence may be underestimated at some of the more trenchward sites (e.g., Eel River), where postseismic

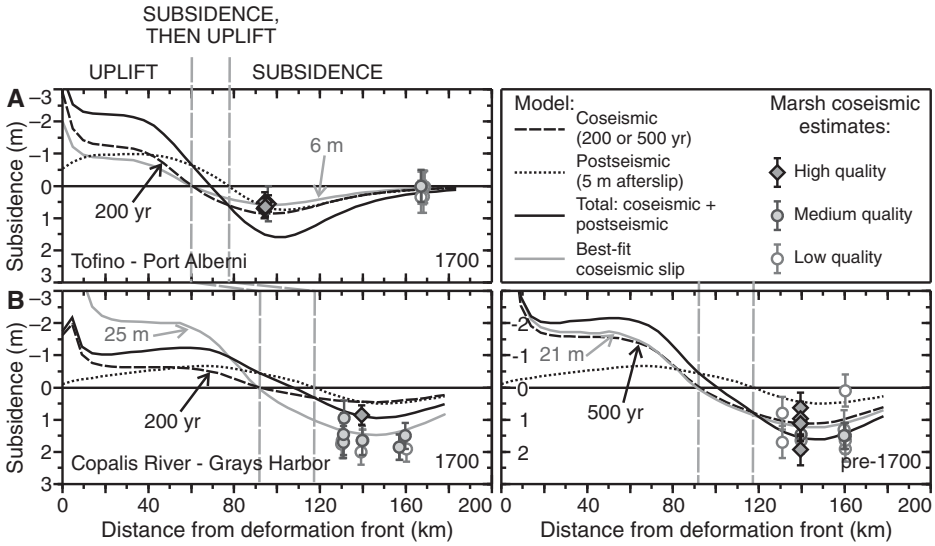

Figure 11. Modeled coseismic, postseismic, and total displacements for comparison with marsh subsidence data for the A.D. 1700 (left) and previous events (right) along two margin-perpendicular profiles (see Fig. 3 for locations A and B). Coseismic deformation (dashed black lines) represents the release of strain accumulated over 200 yr (left; the approximate interval prior to the A.D. 1700 earthquake) or 500 yr (right; mean recurrence interval). Postseismic displacements (dotted lines) are from a preliminary model of afterslip (5 m) on the deep subduction fault. Also shown are the total predicted displacements after both phases (solid black lines), and the coseismic slip model that best fits the weighted mean of the marsh data (solid gray lines).

slip could produce uplift. For the Vancouver Island profile, the combined net displacement predicted at Tofino is a poor match to the marsh data, suggesting that the coseismic estimates are not significantly affected by postseismic deformation. For the Washington profile, contamination of marsh coseismic data by postseismic afterslip could provide an alternative explanation for some of the greater-than-expected subsidence in the A.D. 1700 earthquake. However, very substantial afterslip (~10 m, i.e., more than coseismic slip) would be required to account for all of the extra subsidence, and it is more likely that large coseismic slip played a role, as suggested already. For previous events, a coseismic model consistent with mean recurrence (~500 yr) provides a good fit to the marsh data, although some postseismic influence cannot be ruled out.

This simple model illustrates that postseismic slip may have a significant effect on net vertical deformation at Cascadia coastal sites. Future studies should therefore address the assumption of rapid postevent establishment of marsh elevation indicators. We emphasize that this model is a first-order elastic approximation of the poorly understood processes of postseismic deformation, and further work is required to better constrain the associated temporal variation in surface deformation.

DISCUSSION AND CONCLUSIONS

We have compiled radiocarbon data and estimates of coseismic vertical displacements from buried soil horizons at coastal marsh sites for a 6500 yr history of Cascadia great earthquakes. Event correlations are based on the megathrust earthquake time line determined from the offshore turbidite record by Goldfinger et al. (2003, 2008, 2010). The marsh paleoseismic data lack the resolution to distinguish between single full-margin events and multiple earthquakes occurring over days to decades on shorter segments, but Goldfinger et al.'s turbidite analysis implies synchroneity of rupture during most correlated events, for both full- or near-full-margin earthquakes and shorter ruptures. Dislocation models of segmented rupture predict near-zero coastal coseismic displacements more than ~50 km along strike from the end of a megathrust rupture. Thus, rupture extents inferred from marsh data, where available, should approximately coincide with those inferred from turbidites, which are generated within 90 km of significant shaking (Goldfinger et al., 2007a). Indeed, age-correlated marsh data are compatible with event rupture extents defined by the turbidite record (Goldfinger et al., 2008, 2010).

Comparison between events shows that mean subsidence values are 0.1–0.6 m in coastal southern British Columbia (Vancouver Island; A.D. 1700 event only), 1.0–1.6 m in southern Washington, 0.4–0.9 m in northern Oregon, 0.7–1.2 m in southern Oregon, and 0.7–0.95 m in northern California. Most of the full- or nearly full-margin earthquakes recorded in the sediments, including the most recent great earthquake in A.D. 1700, exhibit subsidence similar to these values. Exceptions include events T2 and 5a, which showed little to no displacement in southern Washington and northern Oregon, and the A.D. 1700 earthquake, which had higher than average subsidence in that region. The consistency of subsidence values among events presently detectable within the data limitations indicates that there is limited variability in rupture behavior between earthquakes, and that hazard analyses based on an average Cascadia event and its uncertainties provide a useful predictor of the subsidence and slip expected in future megathrust earthquakes.

Within the marsh data uncertainties, the coseismic zone of full rupture appears to agree with the downdip width of the interseismic locked zone inferred from geodetic and thermal data, but the subsidence data do not strongly constrain this width. However, at the southern end of the margin, marsh data indicate a zero isobase that is further landward than that predicted by the elastic dislocation model. The model is not designed to account for the complex crustal deformation near the Mendocino triple junction, but the coseismic deformation pattern may be better fit by using a rupture width that is ~25% less than the locked zone inferred from geodetic and thermal data.

Comparisons of the marsh-derived estimates of coseismic subsidence with the predictions of the elastic dislocation models allow estimation of coseismic slip on the megathrust. Modeling results highlight areas where marsh data have the potential to provide the strongest constraints on rupture; this depends on site location relative to the deformation front and rupture zone. For example, a high-precision subsidence estimate (uncertainty ±0.2–0.3 m) provides a better constraint on rupture in southern Oregon than in central Oregon, where low subsidence is expected for a wide range of rupture models (Fig. 7B). Most of the high-precision estimates derived from transfer function analysis (e.g., Hawkes et al., 2008; Nelson et al., 2008) are for sites in northern and central Oregon, where rupture constraints are not optimal (e.g., subsidence of 0.4 ± 0.2 m at Alsea Bay constrains megathrust slip to 20 ± 10 m). The pollen study of Hughes et al. (2002) provides an example of better constraint due to the favorable location of Tofino, Vancouver Island (subsidence of 0.6 ± 0.3 m constrains slip to 6 ± 3 m). Future studies should focus on transfer function analysis of microfossil data sets (diatoms, foraminifera, and/or pollen) to increase the quality and reduce the uncertainty of coseismic subsidence estimates, particularly in areas where better constraints would result, e.g., southern Oregon.

Coseismic slip in the A.D. 1700 earthquake was consistent with the preceding interval of strain accumulation (~200 yr) only at the northern and southern ends of the subduction zone. Elsewhere, the subsidence pattern was closer to an average event, independent of the time since the previous event, i.e., equivalent to the release of strain accumulated over ~500 yr. In southern Washington and northernmost Oregon, greater-than-average slip in A.D. 1700 may indicate a catch-up event to make up for slip deficit in the preceding event T2, but the coseismic subsidence estimates could also include some contamination from postseismic deformation. Strain accumulation of ~200 yr is consistent with the average recurrence in southernmost Cascadia, but it is less than 50% of the average for northernmost Cascadia, where no evidence for megathrust ruptures shorter than full-margin events has been found. Thus, for most of the Cascadia margin, although the coseismic slip is not precisely defined, it appears to be approximately constant from cycle to cycle. In contrast, slip in A.D. 1700 in northernmost Cascadia, which is well defined by high-precision data at Tofino, appears to directly reflect the preceding period of strain buildup. With no quantitative data for previous events, we cannot comment on whether such behavior is typical. Clearly, more work is necessary to better determine the megathrust earthquake history of northernmost Cascadia, incorporating both the timing and, if possible given long-term uplift, coseismic displacements of pre–A.D. 1700 events.

In conclusion, the observed coastal vertical coseismic displacement magnitudes and spatial patterns are reasonably matched by simple elastic dislocation models constrained by geodetic and thermal data and models, although there are important differences in detail. Therefore, the marsh coseismic data support the use of such elastic dislocation models for earthquake rupture and shaking hazard estimation for the Cascadia subduction-zone margin.

ACKNOWLEDGMENTS

We thank Randy Enkin, Chris Goldfinger, Tony Lambert, Garry Rogers, and Kelin Wang for helpful discussions. Thomas Brocher, Ian Hutchinson, Donald White, and an anonymous reviewer provided useful comments that substantially improved the manuscript. Several figures were prepared with the aid of GMT software (Wessel and Smith, 1995). This is Geological Survey of Canada contribution 20090311.

REFERENCES CITED

Adams, J., 1990, Paleoseismicity of the Cascadia subduction zone: Evidence from turbidites off the Oregon-Washington margin: Tectonics, v. 9, p. 569–583, doi: 10.1029/TC009i004p00569.

Atwater, B.F., 1988, Geologic studies for seismic zonation of the Puget lowland, *in* Jacobson, M.L., et al., compilers, National Earthquake Hazards Reduction Program, Summaries of Technical Reports, Volume XXV: U.S. Geological Survey Open-File Report 88–16, p. 120–133.

Atwater, B.F., 1992, Geologic evidence for earthquakes during the past 2000 years along the Copalis River, southern coastal Washington: Journal of Geophysical Research, v. 97, p. 1901–1919, doi: 10.1029/91JB02346.

Atwater, B.F., 1994, Geology of Holocene Liquefaction Features along the Lower Columbia River at Marsh, Brush, Hunting, and Wallace Islands, Oregon and Washington: U.S. Geological Survey Open File Report 94–209, 63 p.

Atwater, B.F., and Hemphill-Haley, E., 1997, Recurrence Intervals for Great Earthquakes of the Past 3,500 Years at Northeastern Willapa Bay, Washington: U.S. Geological Survey Professional Paper 1576, 108 p.

Atwater, B.F., Tuttle, M.P., Schweig, E.S., Rubin, C.M., Yamaguchi, D.K., and Hemphill-Haley, E., 2004a, Earthquake recurrence inferred from paleoseismology, *in* Gillespie A.R., Porter, S.C., and Atwater, B.F., eds., The Quaternary Period in the United States: New York, Elsevier Science, p. 331–350.

Atwater, B.F., Goldfinger, C., and Nelson, C., 2004b, Onshore-offshore correlation of geologic evidence for great Cascadia earthquakes—Permissive agreement between Washington estuaries and Cascadia deep-sea channel: Eos (Transactions, American Geophysical Union), v. 85, no. 47, Fall meeting supplement, abstract T12B–01.

Atwater, B.F., Musumi-Rokkaku, S., Satake, K., Tsuji, Y., Ueda, K., and Yamaguchi, D.K., 2005, The Orphan Tsunami of 1700—Japanese Clues to a Parent Earthquake in North America: U.S. Geological Survey Professional Paper 1707, 144 p.

Banerjee, P., Pollitz, F., Nagarajan, B., and Bürgmann, R., 2007, Coseismic slip distributions of the 26 December 2004 Sumatra-Andaman and 29 March 2005 Nias earthquakes from GPS static offsets: Bulletin of the Seismological Society of America, v. 97, no. 1A, p. S86–S102, doi: 10.1785/0120050609.

Barnett, E.T., 1997, The Potential for Coastal Flooding due to Coseismic Subsidence in the Central Cascadia Margin [M.Sc. thesis]: Portland, Oregon, Portland State University, 144 p.

Bindoff, N.L., Willebrand, J., Artale, V., Cazenave, A., Gregory, J., Gulev, S., Hanawa, K., Le Quéré, C., Levitus, S., Nojiri, Y., Shum, C.K., Talley, L.D., and Unnikrishnan, A., 2007, Observations: Oceanic climate change and sea level, *in* Solomon, S., et al., eds., Climate Change 2007: The Physical Science Basis. Contribution of Working Group I to the Fourth Assessment Report of the Intergovernmental Panel on Climate Change: Cambridge, UK, Cambridge University Press, p. 385–497.

Blais-Stevens, A., Rogers, G.C., and Clague, J.J., 2009, A 4000 year record of earthquakes in the late Holocene sediments from Saanich Inlet, an anoxic fiord near Victoria, British Columbia: Seismological Research Letters, v. 80, no. 2, p. 294.

Briggs, G., 1994, Coastal Crossing of the Zero-Isobase, Cascadia Margin, South-Central Oregon Coast [M.Sc. thesis]: Portland, Oregon, Portland State University, 251 p.

Briggs, G., and Peterson, C.D., 1993, Neotectonics of the Central Cascadia Margin as Recorded on South-Central Oregon Coastal Deposits: U.S. Geological Survey, National Earthquake Hazards Reduction Program, Final Report, 77 p.

Bronk Ramsey, 2001, Development of the radiocarbon calibration program OxCal: Radiocarbon, v. 43, p. 355–363.

Brudzinski, M.R., and Allen, R.M., 2007, Segmentation in episodic tremor and slip all along Cascadia: Geology, v. 35, no. 10, p. 907–910, doi: 10.1130/G23740A.1.

Carver, G., and Burke, R.B., 1989, Active convergent tectonics in northwestern California, *in* Aalto, K.R., et al., eds., Geological Evolution of the Northernmost Coast Ranges and Western Klamath Mountains, California: Washington, DC, American Geophysical Union, Field Trip Guidebook T308, 28th International Geologic Congress, p. 64–82.

Carver, G.A., Stuiver, M., and Atwater, B.F., 1992, Radiocarbon ages of earthquake-killed trees at Humboldt Bay, California [abs.]: Eos (Transactions, American Geophysical Union), Fall meeting supplement, v. 73, p. 398.

Carver, G., Jayko, A.S., Valentine, D.W., and Li, W.H., 1994, Coastal uplift associated with the 1992 Cape Mendocino earthquake, northern California: Geology, v. 22, p. 195–198, doi: 10.1130/0091-7613(1994)022<0195:CUAWTC>2.3.CO;2.

Chaytor, J.D., Goldfinger, C., Dziak, R.P., and Fox, C.G., 2004, Active deformation of the Gorda plate: Constraining deformation models with new geophysical data: Geology, v. 32, no. 4, p. 353–356, doi: 10.1130/G20178.2.

Cherniawsky, J.Y., Titov, V.V., Wang, K., and Li, J.-Y., 2007, Numerical simulations of tsunami waves and currents for southern Vancouver Island from a Cascadia megathrust earthquake: Pure and Applied Geophysics, v. 164, p. 465–492, doi: 10.1007/s00024-006-0169-0.

Chlieh, M., Avouac, J.-P., Hjorleifsdottir, V., Song, T.-R.A., Ji, C., Sieh, K., Sladen, A., Hebert, H., Prawirodirdjo, L., Bock, Y., and Galetzka, J., 2007, Coseismic slip and afterslip of the great M_W 9.15 Sumatra-Andaman earthquake of 2004: Bulletin of the Seismological Society of America, v. 97, p. S152–S173, doi: 10.1785/0120050631.

Cisternas, M., Atwater, B.F., Torrejón, F., Sawai, Y., Machuca, G., Lagos, M., Eipert, A., Youlton, C., Salgado, I., Kamataki, T., Shishikura, M., Rajendran, C.P., Malik, J.K., Rizal, Y., and Husni, M., 2005, Predecessors of the giant 1960 Chile earthquake: Nature, v. 437, no. 15, p. 404–407, doi: 10.1038/nature03943.

Clague, J.J., and Bobrowsky, P.T., 1994a, Tsunami deposits in tidal marshes on Vancouver Island, British Columbia: Geological Society of America Bulletin, v. 106, p. 1293–1303, doi: 10.1130/0016-7606(1994)106<1293:TDBTMO>2.3.CO;2.

Clague, J.J., and Bobrowsky, P.T., 1994b, Evidence for a large earthquake and tsunami 100–400 years ago on western Vancouver Island, British Columbia: Quaternary Research, v. 41, p. 176–184, doi: 10.1006/qres.1994.1019.

Clague, J.J., Hutchinson, I., Mathewes, R.W., and Patterson, R.T., 1999, Evidence for late Holocene tsunamis at Catala Lake, British Columbia: Journal of Coastal Research, v. 15, no. 1, p. 45–60.

Clague, J.J., Bobrowsky, P.T., and Hutchinson, I., 2000, A review of geological records of large tsunamis at Vancouver Island, British Columbia, and implications for hazard: Quaternary Science Reviews, v. 19, p. 849–863, doi: 10.1016/S0277-3791(99)00101-8.

Clarke, S.H., and Carver, G.A., 1992, Late Holocene tectonics and paleoseismicity, southern Cascadia subduction zone: Science, v. 255, p. 188–192, doi: 10.1126/science.255.5041.188.

Darienzo, M.E., 1991, Late Holocene Paleoseismicity along the Northern Oregon Coast [Ph.D. thesis]: Portland, Oregon, Portland State University, 176 p.

Darienzo, M.E., and Peterson, C.D., 1990, Episodic tectonic subsidence of late Holocene salt marshes, northern Oregon, central Cascadia margin: Tectonics, v. 9, p. 1–22, doi: 10.1029/TC009i001p00001.

Darienzo, M.E., and Peterson, C.D., 1995, Magnitude and frequency of subduction-zone earthquakes along the northern Oregon coast in the past 3,000 years: Oregon Geology, v. 57, p. 3–12.

Darienzo, M.E., Peterson, C.D., and Clough, C., 1994, Stratigraphic evidence for great subduction-zone earthquakes at four estuaries in northern Oregon, U.S.A.: Journal of Coastal Research, v. 10, no. 4, p. 850–876.

Dragert, H., Hyndman, R.D., Rogers, G.C., and Wang, K., 1994, Current deformation and the width of the seismogenic zone of the northern Cascadia subduction thrust: Journal of Geophysical Research, v. 99, p. 653–668, doi: 10.1029/93JB02516.

Flück, P., Hyndman, R.D., and Wang, K., 1997, Three-dimensional dislocation model for great earthquakes of the Cascadia subduction zone: Journal of Geophysical Research, v. 102, no. 9, p. 20,539–20,550, doi: 10.1029/97JB01642.

Friele, P.A., and Hutchinson, I., 1993, Holocene sea-level change on the central-west coast of Vancouver Island, British Columbia: Canadian Journal of Earth Sciences, v. 30, p. 832–840, doi: 10.1139/e93-069.

Gahalaut, V.K., Jade, S., Catherine, J.K., Gireesh, R., Ananda, M.B., Dileep Kumar, P., Narsaiah, M., Jafri, S.S.H., Ambikapathy, A., Bansal, A., Chadha, R.K., Gupta, D.C., Nagarajan, B., and Kumar, S., 2008, GPS measurements of postseismic deformation in the Andaman-Nicobar region following the giant 2004 Sumatra-Andaman earthquake: Journal of Geophysical Research, v. 113, doi: 10.1029/2007JB005511.

Garrison-Laney, C.E., Abramson-Ward, H.F., and Carver, G., 2006, A 3,000 year record of tsunami deposition from the southern end of the Cascadia subduction zone, *in* Hemphill-Haley, M., Leroy, T., McPherson, B., Patton, J., Stallman J., Sutherland, D., and Williams, T., eds., Signatures of Quaternary crustal deformation and landscape evolution in the Mendocino deformation zone, NW California: Pacific Cell Friends of the Pleistocene 2006 Guidebook, Paper 4–2-A, p. 309–323.

Geist, E.L., 2005, Local Tsunami Hazards in the Pacific Northwest from Cascadia Subduction Zone Earthquakes: U.S. Geological Survey Professional Paper 1661-B, 17 p.

Goldfinger, C., Nelson, C.H., Johnson, J.E., and the Shipboard Scientific Party, 2003, Holocene earthquake records from the Cascadia subduction zone and northern San Andreas fault based on precise dating of offshore turbidites: Annual Review of Earth and Planetary Sciences, v. 31, p. 555–577, doi: 10.1146/annurev.earth.31.100901.141246.

Goldfinger, C., Morey, A.E., Nelson, C.H., Gutierrez-Pastor, J., Johnson, J.E., Karabanov, E., Chaytor, J., and Ericsson, A., 2007a, Rupture lengths and temporal history of significant earthquakes on the offshore and north coast segments of the northern San Andreas fault based on turbidite stratigraphy: Earth and Planetary Science Letters, v. 254, p. 9–27, doi: 10.1016/j.epsl.2006.11.017.

Goldfinger, C., Wang, K., Witter, R., Baptista, A., Zhang, Y., Priest, G., Nelson, H., Morey, A., and Johnson, J., 2007b, Interplay of structure and sediment supply may influence subduction zone rupture patches and propagation [abs.]: Eos (Transactions, American Geophysical Union), Fall meeting supplement, v. 88, no. 52, abstract T52A–07.

Goldfinger, C., Grijalva, K., Bürgmann, R., Morey, A.E., Johnson, J.E., Nelson, H., Gutiérrez-Pastor, J., Ericsson, A., Karabanov, E., Chaytor, J.D., Patton, J., and Gràcia, E., 2008, Late Holocene rupture of the northern San Andreas fault and possible stress linkage to the Cascadia subduction zone: Bulletin of the Seismological Society of America, v. 98, no. 2, p. 861–889, doi: 10.1785/0120060411.

Goldfinger, C., Nelson, C.H., Johnson, J.E., Morey, A.E., Gutiérrez-Pastor, J., Karabanov, E., Eriksson, A.T., Gràcia, E., Dunhill, G., Patton, J., Enkin, R., Dallimore, A., and Vallier, T., and the Shipboard Scientific Parties, 2010, Turbidite Event History: Methods and Implications for Holocene Paleoseismicity of the Cascadia Subduction Zone: U.S. Geological Survey Professional Paper 1661-F (in press).

Guilbault, J.P., Clague, J.J., and Lapointe, M., 1995, Amount of subsidence during a late Holocene earthquake—Evidence from fossil tidal marsh foraminifera at Vancouver Island, west coast of Canada: Palaeogeography, Palaeoclimatology, Palaeoecology, v. 118, p. 49–71, doi: 10.1016/0031-0182(94)00135-U.

Guilbault, J.P., Clague, J.J., and Lapointe, M., 1996, Foraminifera evidence for the amount of coseismic subsidence during a late Holocene earthquake on Vancouver Island, west coast of Canada: Quaternary Science Reviews, v. 15, p. 913–937, doi: 10.1016/S0277-3791(96)00058-3.

Hanks, T.C., and Kanamori, H., 1979, A moment magnitude scale: Journal of Geophysical Research, v. 84, p. 2348–2350, doi: 10.1029/JB084iB05p02348.

Hawkes, A.D., Scott, D.B., Lipps, J.H., and Combellick, R., 2005, Evidence for possible precursor events of megathrust earthquakes on the west coast of North America: Geological Society of America Bulletin, v. 117, no. 7/8, p. 996–1008, doi: 10.1130/B25455.1.

Hawkes, A.D., Horton, B.P., Nelson, A.R., and Grand Pre, C., 2008, Late Holocene coseismic deformation at the Cascadia subduction zone, Oregon, USA [abs.]: Eos (Transactions, American Geophysical Union), Fall meeting supplement, v. 89, no. 53, abstract T53B–1937.

Hemphill-Haley, E., 1995, Diatom evidence for earthquake-induced subsidence and tsunami 300 yr ago in southern coastal Washington: Geological Society of America Bulletin, v. 107, p. 367–378, doi: 10.1130/0016-7606(1995)107<0367:DEFEIS>2.3.CO;2.

Hsu, Y.-J., Simons, M., Avouac, J.-P., Galetzka, J., Sieh, K., Chlieh, M., Natawidjaja, D., Prawirodirdjo, L., and Bock, Y., 2006, Frictional afterslip following the 2005 Mias-Simeulue earthquake, Sumatra: Science, v. 312, p. 1921–1926, doi: 10.1126/science.1126960.

Hughes, J.F., Mathewes, R.W., and Clague, J.J., 2002, Use of pollen and vascular plants to estimate coseismic subsidence at a tidal marsh near Tofino, British Columbia: Palaeogeography, Palaeoclimatology, Palaeoecology, v. 185, p. 145–161, doi: 10.1016/S0031-0182(02)00283-3.

Hutchinson, I., Clague, J.J., and Mathewes, R.W., 1997, Reconstructing the tsunami record on an emerging coast: A case study of Kanim Lake, Vancouver Island, British Columbia, Canada: Journal of Coastal Research, v. 13, no. 2, p. 545–553.

Hutchinson, I., Guilbault, J.P., Clague, J.J., and Bobrowsky, P.T., 2000, Tsunamis and tectonic deformation at the northern Cascadia margin; a 3000-year record from Deserted Lake, Vancouver Island, British Columbia, Canada: The Holocene, v. 10, no. 4, p. 429–439, doi: 10.1191/095968300666654539.

Hutton, W., DeMets, C., Sanchez, O., Suarez, G., and Stock, J., 2001, Slip kinematics and dynamics during and after the 1995 October 9 M_w-8.0 Colima-Jalisco earthquake, Mexico, from GPS geodetic constraints: Geophysical Journal International, v. 146, p. 637–658, doi: 10.1046/j.1365-246X.2001.00472.x.

Hyndman, R.D., and Wang, K., 1993, Thermal constraints on the zone of major thrust earthquake failure: The Cascadia subduction zone: Journal of Geophysical Research, v. 98, no. B2, p. 2039–2060, doi: 10.1029/92JB02279.

Hyndman, R.D., and Wang, K., 1995, The rupture zone of Cascadia great earthquakes from current deformation and the thermal regime: Journal of Geophysical Research, v. 100, p. 22,133–22,154, doi: 10.1029/95JB01970.

Hyndman, R.D., Leonard, L.J., and Currie, C.A., 2005, Test of Models for the Cascadia Great Earthquake Rupture Area Using Coastal Subsidence Estimates for the 1700 Earthquake: U.S. Geological Survey NEHRP External Grant Award 04HQGR0088, Final Report, 11 p.

Jacoby, G.C., Carver, G.A., and Wagner, W., 1995, Trees and herbs killed by an earthquake 300 yr ago at Humboldt Bay, California: Geology, v. 23, p. 77–80, doi: 10.1130/0091-7613(1995)023<0077:TAHKBA>2.3.CO;2.

Kao, H., Shan, S.-J., Dragert, H., Rogers, G., Cassidy, J.F., Wang, K., James, T.S., and Ramachandran, K., 2006, Spatial-temporal patterns of seismic tremors in northern Cascadia: Journal of Geophysical Research, v. 111, p. B03309, doi: 10.1029/2005JB003727.

Kelsey, H.M., Witter, R.C., and Hemphill-Haley, E., 1998, Response of a small Oregon estuary to coseismic subsidence and postseismic uplift in the past 300 years: Geology, v. 26, no. 3, p. 231–234, doi: 10.1130/0091-7613(1998)026<0231:ROASOE>2.3.CO;2.

Kelsey, H.M., Witter, R.C., and Hemphill-Haley, E., 2002, Plate-boundary earthquakes and tsunamis of the past 5500 yr, Sixes River estuary, southern Oregon: Geological Society of America Bulletin, v. 114, no. 3, p. 298–314, doi: 10.1130/0016-7606(2002)114<0298:PBEATO>2.0.CO;2.

Kelsey, H.M., Nelson, A.R., Hemphill-Haley, E., and Witter, R.C., 2005, Tsunami history of an Oregon coastal lake reveals a 4600 yr record of great earthquakes on the Cascadia subduction zone: Geological Society of America Bulletin, v. 117, no. 7/8, p. 1009–1032, doi: 10.1130/B25452.1.

Lay, T., and Kanamori, H., 1980, Earthquake doublets in the Solomon Islands: Physics of the Earth and Planetary Interiors, v. 21, no. 4, p. 283–304, doi: 10.1016/0031-9201(80)90134-X.

Leonard, L.J., Hyndman, R.D., and Mazzotti, S., 2004, Coseismic subsidence in the 1700 great Cascadia earthquake: Coastal estimates versus elastic dislocation models: Geological Society of America Bulletin, v. 116, p. 655–670, doi: 10.1130/B25369.1.

Li, W.H., 1992, Late Holocene Paleoseismology in the Lower Eel River Valley, Northern California [M.Sc. thesis]: Arcata, California, Humboldt State University, 78 p.

Ludwin, R.S., Dennis, R., Carver, D., McMillan, A.D., Losey, R., Clague, J., Jonientz-Trisler, C., Bowechop, J., Wray, J., and James, K., 2005, Dating the 1700 Cascadia earthquake: Great coastal earthquakes in Native stories: Seismological Research Letters, v. 76, no. 2, p. 140–148, doi: 10.1785/gssrl.76.2.140.

Mathewes, R.W., and Clague, J.J., 1994, Detection of large prehistoric earthquakes in the Pacific Northwest by microfossil analysis: Science, v. 264, p. 688–691, doi: 10.1126/science.264.5159.688.

Mazzotti, S., Dragert, H., Henton, J., Schmidt, M., Hyndman, R., James, T., Lu, Y., and Craymer, M., 2003, Current tectonics of northern Cascadia from a decade of GPS measurements: Journal of Geophysical Research, v. 108, no. B12, p. 2554, doi: 10.1029/2003JB002653.

McCaffrey, R., Long, M.D., Goldfinger, C., Zwick, P.C., Nabelek, J.L., Johnson, C.K., and Smith, C., 2000, Rotation and plate locking at the southern Cascadia subduction zone: Geophysical Research Letters, v. 27, no. 19, p. 3117–3120, doi: 10.1029/2000GL011768.

McCaffrey, R., Qamar, A.I., King, R.W., Wells, R., Khazaradze, G., Williams, C.A., Stevens, C.W., Vollick, J.J., and Zwick, P.C., 2007, Fault locking, block rotation and crustal deformation in the Pacific Northwest: Geophysical Journal International, v. 169, no. 3, p. 1315–1340, doi: 10.1111/j.1365-246X.2007.03371.x.

McCann, W.R., Pérez, O.J., and Sykes, L.R., 1980, Yakataga gap, Alaska: Seismic history and earthquake potential: Science, v. 207, p. 1309–1314.

Melbourne, T.I., Webb, F.H., Stock, J.M., and Reigber, C., 2002, Rapid postseismic transients in subduction zones from continuous GPS: Journal of Geophysical Research, v. 107, doi: 10.1029/2001JB000555.

Merritts, D.J., 1996, The Mendocino triple junction: Active faults, episodic coastal emergence, and rapid uplift: Journal of Geophysical Research, v. 101, p. 6051–6070, doi: 10.1029/95JB01816.

Minor, R., and Grant, W.C., 1996, Earthquake-induced subsidence and burial of late Holocene archaeological sites, northern Oregon coast: American Antiquity, v. 61, no. 4, p. 772–781, doi: 10.2307/282017.

Nakanishi, A., Takahashi, N., Park, J.-O., Miura, S., Kodaira, S., Kaneda, Y., Hirata, N., Iwasaki, T., and Nakamura, M., 2002, Crustal structure across the coseismic rupture zone of the 1944 Tonankai earthquake, the central Nankai Trough seismogenic zone: Journal of Geophysical Research, v. 107, no. B1, doi: 10.1029/2001JB000424.

Nelson, A.R., 1992a, Holocene tidal-marsh stratigraphy in south-central Oregon—Evidence for localized sudden submergence in the Cascadia subduction zone, *in* Fletcher, C.H., III, et al., eds., Quaternary Coasts of the United States: Marine and Lacustrine Systems: Society for Sedimentary Geology Special Publication 48, p. 287–301.

Nelson, A.R., 1992b, Discordant ^{14}C ages from buried tidal-marsh soils in the Cascadia subduction zone, southern Oregon coast: Quaternary Research, v. 38, p. 74–90, doi: 10.1016/0033-5894(92)90031-D.

Nelson, A.R., Shennan, I., and Long, A.J., 1996a, Identifying coseismic subsidence in tidal-wetland stratigraphic sequences at the Cascadia subduction zone of western North America: Journal of Geophysical Research, v. 101, no. B3, p. 6115–6135, doi: 10.1029/95JB01051.

Nelson, A.R., Jennings, A.E., and Kashima, K., 1996b, An earthquake history derived from stratigraphic and microfossil evidence of relative sea-level change at Coos Bay, southern coastal Oregon: Geological Society of America Bulletin, v. 108, p. 141–154, doi: 10.1130/0016-7606(1996)108<0141:AEHDFS>2.3.CO;2.

Nelson, A.R., Ota, Y., Umitsu, M., Kashima, K., and Matsushima, Y., 1998, Seismic or hydrodynamic control of rapid late-Holocene sea-level rises in southern coastal Oregon, USA: The Holocene, v. 8, no. 3, p. 287–299, doi: 10.1191/095968398668600476.

Nelson, A.R., Asquith, A.C., and Grant, W.C., 2004, Great earthquakes and tsunamis of the past 2000 years at the Salmon River estuary, central Oregon coast, USA: Bulletin of the Seismological Society of America, v. 94, no. 4, p. 1276–1292, doi: 10.1785/012003210.

Nelson, A.R., Kelsey, H.M., and Witter, R.C., 2006, Great earthquakes of variable magnitude at the Cascadia subduction zone: Quaternary Research, v. 65, p. 354–365, doi: 10.1016/j.yqres.2006.02.009.

Nelson, A.R., Sawai, Y., Jennings, A.E., Bradley, L.-A., Gerson, L., Sherrod, B.L., Sabean, J., and Horton, B.P., 2008, Great-earthquake paleogeodesy and tsunamis of the past 2000 years at Alsea Bay, central Oregon coast, USA: Quaternary Science Reviews, v. 27, p. 747–768, doi: 10.1016/j.quascirev.2008.01.001.

Olsen, K.B., Stephenson, W.J., and Geisselmeyer, A., 2008, 3D crustal structure and long-period ground motions from a M9.0 megathrust earthquake in the Pacific Northwest region: Journal of Seismology, v. 12, no. 2, p. 145–159, doi: 10.1007/s10950-007-9082-y.

Ovenshine, A.T., and Kachadoorian, R., 1976, Estimate of time required for natural restoration of the effects of the 1964 earthquake at Portage, *in* Cobb, E.H., ed., The U.S. Geological Survey in Alaska: Accomplishments during 1975: U.S. Geological Survey Circular 733, p. 53–54.

Patton, J.R., and Witter, R.C., 2006, Late Holocene coseismic subsidence and coincident tsunamis, southern Cascadia subduction zone, Hookton Slough, Wigi (Humboldt Bay), California, *in* Hemphill-Haley, M., Leroy, T., McPherson, B., Patton, J., Stallman J., Sutherland, D., and Williams, T., eds., Signatures of Quaternary crustal deformation and landscape evolution in the Mendocino deformation zone, NW California: Pacific Cell Friends of the Pleistocene 2006 Guidebook, Paper 2–3-B, p. 181–193.

Paul, J., Lowry, A.R., Bilham, R., Sen, S., and Smalley, R., Jr., 2007, Postseismic deformation of the Andaman Islands following the 26 December, 2004 Great Sumatra-Andaman earthquake: Geophysical Research Letters, v. 34, doi: 10.1029/2007GL031024.

Peters, R., Jaffe, B., Gelfenbaum, G., and Peterson, C., 2003, Cascadia Tsunami Deposit Database: U.S. Geological Survey Open-File Report 03–13, 24 p.

Peterson, C.D., and Darienzo, M.E., 1989, Episodic, abrupt tectonic subsidence recorded in late Holocene deposits of the South Slough syncline: An on-land expression of shelf fold belt deformation from the southern Cascadia margin: Geological Society of America Abstracts with Programs, v. 21, no. 5, p. 129.

Peterson, C.D., and Darienzo, M.E., 1991, Discrimination of Climatic, Oceanic and Tectonic Mechanisms of Cyclic Marsh Burial from Alsea Bay, Oregon, U.S.A.: U.S. Geological Survey Open-File Report 91–441-C, 53 p.

Peterson, C.D., and Madin, I.P., 1997, Coseismic paleoliquefaction evidence in the central Cascadia margin, USA: Oregon Geology, v. 59, no. 3, p. 51–74.

Peterson, C.D., and Priest, G.R., 1995, Preliminary reconnaissance of Cascadia paleotsunami deposits in Yaquina Bay, Oregon: Oregon Geology, v. 57, p. 33–40.

Peterson, C.D., Darienzo, M.E., Burns, S.F., and Burris, W., 1993, Field trip guide to Cascadia paleoseismic evidence along the northern Oregon coast: Evidence of subduction zone paleoseismicity in the central Cascadia margin: Oregon Geology, v. 55, p. 99–114.

Peterson, C.D., Darienzo, M.E., Doyle, D., and Barnett, E., 1996, Evidence for coseismic subsidence and tsunami deposition during the past 3,000 years at Siletz Bay, Oregon, *in* Priest, G.R., ed., Explanation of Mapping Methods and Use of the Tsunami Hazard Map of the Siletz Bay Area, Lincoln City, Oregon: Oregon Department of Geology and Mineral Industries Open-File Report 0–95–5, 25 p.

Peterson, C.D., Barnett, E.T., Briggs, G.C., Carver, G.A., Clague, J.J., and Darienzo, M.E., 1997, Estimates of

Coastal Subsidence from Great Earthquakes in the Cascadia Subduction Zone, Vancouver Island, B.C., Washington, Oregon, and Northernmost California: State of Oregon, Department of Geology and Mineral Industries Open-File Report O-97-05, 44 p.

Peterson, C.D., Doyle, D.L., and Barnett, E.T., 2000, Coastal flooding and beach retreat from coseismic subsidence in the central Cascadia margin, USA: Environmental & Engineering Geoscience, v. 6, p. 255–269.

Pritchard, C.J., 2004, Late Holocene Relative Sea-Level Changes, Arcata Bay, California: Evaluation of Freshwater Syncline Movement Using Coseismically Buried Soil Horizons [Master's thesis]: Arcata, California, Humboldt State University, 64 p.

Reimer, P.J., Baillie, M.G.L., Bard, E., Bayliss, A., Beck, J.W., Bertrand, C.J.H., Blackwell, P.G., Buck, C.E., Burr, G.S., Cutler, K.B., Damon, P.E., Edwards, R.L., Fairbanks, R.G., Friedrich, M., Guilderson, T.P., Hogg, A.G., Hughen, K.A., Kromer, B., McCormac, G., Manning, S., Bronk Ramsey, C., Reimer, R.W., Remmele, S., Southon, J.R., Stuiver, M., Talamo, S., Taylor, F.W., van der Plicht, J., and Weyhenmeyer, C.E., 2004, IntCal04 terrestrial radiocarbon age calibration, 0–26 cal kyr BP: Radiocarbon, v. 46, no. 3, p. 1029–1058.

Sabean, J.A.R., 2004, Applications of Foraminifera to Detecting Land Level Change Associated with Great Earthquakes along the West Coast of North America [M.Sc. thesis]: Burnaby, British Columbia, Simon Fraser University, 90 p.

Satake, K., Shimazaki, K., Tsuji, Y., and Ueda, K., 1996, Time and size of a giant earthquake in Cascadia inferred from Japanese tsunami records of January 1700: Nature, v. 379, p. 246–249, doi: 10.1038/379246a0.

Satake, K., Wang, K., and Atwater, B.F., 2003, Fault slip and seismic moment of the 1700 Cascadia earthquake inferred from Japanese tsunami descriptions: Journal of Geophysical Research, v. 108, no. B11, p. 2535, doi: 10.1029/2003JB002521.

Shennan, I., and Hamilton, S., 2006, Coseismic and preseismic subsidence associated with great earthquakes in Alaska: Quaternary Science Reviews, v. 25, p. 1–8, doi: 10.1016/j.quascirev.2005.09.002.

Shennan, I., Long, A.J., Rutherford, M.M., Green, F.M., Innes, J.B., Lloyd, J.M., Zong, Y., and Walker, K.J., 1996, Tidal marsh stratigraphy, sea-level change and large earthquakes: I. A 5000 year record in Washington, USA: Quaternary Science Reviews, v. 15, p. 1023–1059, doi: 10.1016/S0277-3791(96)00007-8.

Shennan, I., Long, A.J., Rutherford, M.M., Innes, J.B., Green, F.M., and Walker, K.J., 1998, Tidal marsh stratigraphy, sea-level change and large earthquakes: II. Submergence events during the last 3500 years at Netarts Bay, Oregon, USA: Quaternary Science Reviews, v. 17, p. 365–393, doi: 10.1016/S0277-3791(97)00055-3.

Turcotte, D.L., and Schubert, G., 2002, Geodynamics: Cambridge, UK, Cambridge University Press, 456 p.

Valentine, D.W., 1992, Late Holocene Stratigraphy, Humboldt Bay, California: Evidence for Late Holocene Paleoseismicity of the Southern Cascadia Subduction Zone [Master's thesis]: Arcata, California, Humboldt State University, 84 p.

Vick, G.S., 1988, Late Holocene Paleoseismicity and Relative Sea Level Changes of the Mad River Slough, Northern Humboldt Bay, California [Master's thesis]: Arcata, California, Humboldt State University, 87 p.

Wang, K., 2007, Elastic and viscoelastic models for subduction earthquake cycles, *in* Dixon, T.H., and Moore, S.C., eds., The Seismogenic Zone of Subduction Thrust Faults: New York, Columbia University Press, p. 540–575.

Wang, K., and He, J., 2008, Effects of frictional behavior and geometry of subduction fault on coseismic seafloor deformation: Bulletin of the Seismological Society of America, v. 98, no. 2, p. 571–579, doi: 10.1785/0120070097.

Wang, K., and Rogers, G.C., 1994, An explanation for the double seismic layers north of the Mendocino triple junction: Geophysical Research Letters, v. 21, no. 2, p. 121–124, doi: 10.1029/93GL03538.

Wang, K., Wells, R., Mazzotti, S., Hyndman, R.D., and Sagiya, T., 2003, A revised dislocation model of interseismic deformation of the Cascadia subduction zone: Journal of Geophysical Research, v. 108, no. B1, doi: 10.1029/2001JB001227.

Wells, R.E., and Simpson, R.W., 2001, Northward migration of the Cascadia forearc in the northwestern US and implications for subduction deformation: Earth, Planets, and Space, v. 53, no. 4, p. 275–283.

Wessel, P., and Smith, W.H.F., 1995, New version of the Generic Mapping Tools released: Eos (Transactions, American Geophysical Union), v. 76, p. F329, doi: 10.1029/95EO00198.

Williams, H.F.L., Hutchinson, I., and Nelson, A.R., 2005, Multiple sources for late-Holocene tsunamis at Discovery Bay, Washington State, USA: The Holocene, v. 15, no. 1, p. 60–73, doi: 10.1191/0956683605hl784rp.

Witter, R.C., Kelsey, H.M., and Hemphill-Haley, E., 1997, A Paleoseismic History of the South-Central Cascadia Subduction Zone; Assessing Earthquake Recurrence Intervals and Upper-Plate Deformation over the Past 6600 Years at the Coquille River Estuary, Southern Oregon, U.S.A.: U.S. Geological Survey National Earthquake Hazards Reduction Program External Grant Award 1434-HQ-97-GR-03036, Final Report, 54 p.

Witter, R.C., Kelsey, H.M., and Hemphill-Haley, E., 2003, Great Cascadia earthquakes and tsunamis of the past 6700 years, Coquille River estuary, southern coastal Oregon: Geological Society of America Bulletin, v. 115, no. 10, p. 1289–1306, doi: 10.1130/B25189.1.

Yamaguchi, D.K., Atwater, B.F., Bunker, D.E., Benson, B.E., and Reid, M.S., 1997, Tree-ring dating the 1700 Cascadia earthquake: Nature, v. 389, p. 922–923, doi: 10.1038/40048.

Zweck, C., Freymueller, J.T., and Cohen, S.C., 2002, Three-dimensional elastic dislocation modelling of the postseismic response to the 1964 Alaska earthquake: Journal of Geophysical Research, v. 107, no. B4, p. 2064, doi: 10.1029/2001JB000409.

Manuscript Received 18 June 2009
Revised Manuscript Received 19 September 2009
Manuscript Accepted 14 October 2009

Printed in the USA